Emergent Materials (2021) 4:1093–1124
https://doi.org/10.1007/s42247-021-00262-x

REVIEW

Two is better than one: catalytic, sensing and optical applications of doped zinc oxide nanostructures

Viswanathan Vinitha[1] · Mani Preeyanghaa[2] · Vasudevan Vinesh[2] · Ravikumar Dhanalakshmi[1] · Bernaurdshaw Neppolian[2] · Vajiravelu Sivamurugan[1]

Received: 31 May 2021 / Accepted: 3 July 2021 / Published online: 17 August 2021

Abstract

Nanosized ZnO-based materials for catalytic and sensing applications are highly proficient over bulk catalytic analogous due to higher surface and tunable physicochemical properties. The functionality, porosity, shape, size and surface area of these nanomaterials are crucial factors for influencing specificity and efficiency of its applications. In this review, we contemplated the effect of metal doping on ZnO nanoparticles for various applications such as solar cells, photocatalysis, medicines, light-emitting diodes, laser diodes, chemical and biosensors. The potential applications of metal-doped ZnO have gained significant attention owing to direct influence by the dopants on electronic and physiochemical properties. Especially, the natural bandgap (3.37 eV) and n-type conducting behaviour of ZnO can be tuned by doping of metals/metal oxides and non-metals by replacing Zn^{2+} and O^{2-} in ZnO lattices respectively. Further, the bandgap modified ZnO could be used as a multi-functional material by growing it in various nanostructures such as bulk, thin layer and wires.

1 Introduction

Nanostructured pure and doped metal oxides play a pivotal place in the fabrication of solar cells, catalysis, energy conversion, energy storage, data storage, optoelectronic, bioimaging, magnetic, sensing, theragnostic, environmental, automobile and personal safety applications. Over the period of time, the applications of inorganic metal oxide nanomaterials have been thoroughly studied [1–4]. On the other hand, the commercial and real-time utilization of the metal oxides-based devices could be limited due to availability and cost effectiveness of the metal oxides. Among the widely explored metal oxides, ZnO is found to be in the top of list because of its functional versatility, simple synthetic method, tunable properties, availability and primarily cost effective. For more than two decades, ZnO-based nanomaterials have been widely explored for many applications such as sensor, bioimaging, theragnostic, photocatalytic and energy conversion applications [5–8] (Figure 1). Zinc oxide (ZnO) is a unique material when compared with other metal oxides, ZnO can deliver advantages like cost-effectiveness, larger specific surface area, higher pore volume and variable engineering nanostructured properties [9]. The major advantage of ZnO nanoparticles over others is their tunable bandgap and particle size, which makes it applicable in many areas. Especially, in biological study including anti-microbial, the photocatalytic and semiconducting behaviour make it as anticancer drugs for new generation early diagnosis, treatment and nano-antibiotics [10]. In addition, ZnO is proven to be the best adsorbent for the removal of organic pollutants such as pharmaceuticals and pesticides from industrial wastewater effluent [11].

However, ZnO nanoparticles have shown limited photo stability in the biological environment and have unexpected cytotoxic effects. To circumvent the above-mentioned setbacks, doping of ZnO with metal/non-metal seems to be one of the viable and simple solutions due to the occurrence of wide spectrum of dopants [12]. Doping means intentionally introducing impurities, i.e. introducing metal ions into the crystal structure of ZnO to enhance or suppress any kind of

✉ Bernaurdshaw Neppolian
neppolib@srmist.edu.in

✉ Vajiravelu Sivamurugan
sivaatnus@gmail.com

[1] PG and Research Department of Chemistry, Pachaiyappa's College, 600 030, Chennai, India

[2] Department of Physics and Nanotechnology & SRM Research Institute, SRM Institute of Science and Technology, Kattankulathur, Chennai 603203, India

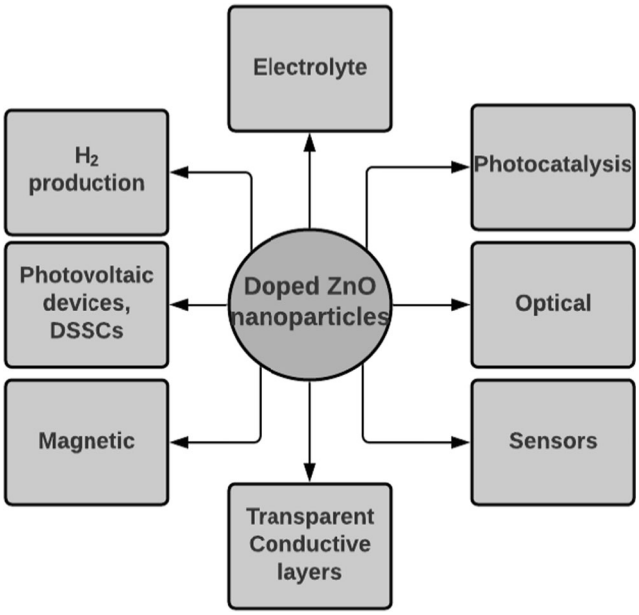

Fig. 1 Multi-functional applications of doped ZnO nanoparticles

physicochemical properties of the ZnO. Doping is mainly of two types typically known as cationic and the other is of anionic doping, which replaces Zn^{2+} and O^{2-} in the crystal lattice respectively. The introduction of cationic impurities into the ZnO structure is known as cationic doping most prominently transition metals/rare earths are used as cationic dopants, e.g. Sn^{4+}, Al^{3+}, Ga^{3+}, In^{3+}, Cd^{2+}, Cu^{2+}, Mn^{2+}, Ni^{2+}, La^{3+}, Eb^{3+} and Gd^{3+} ions. The doping of anion into the ZnO is called anionic doping, e.g. As, N, S are anionic dopants, which predominantly make ZnO as p-type conducting material [9, 13]. The main purpose of choosing doped ZnO nanostructure is due to its cost-effective sol-gel, hydrothermal and co-precipitation synthetic procedure and its technological applications, and it can be grown in thinfilms, nanowires and nanorods. The main reason for its wide technological application is belonging to its physical and chemical properties [5, 13–15]. For more than two decades, ZnO nanoparticles are well known for their photocatalytic applications. The role of dopants plays a major role of fine tuning the electronic behaviour of ZnO, which makes it a versatile material for applications in sensor, optical, light-emitting diodes, photovoltaic, photodetectors, magnetic, H_2 production including anti-microbial etc. Type and level of doping, especially metal ions doped on ZnO lattices, altered electronic properties of ZnO, which showed direct impact on their functional behaviour. The review encompasses the latest developments in bandgap modification of ZnO through doping transition and non-metals-doped zinc oxide having variable nanostructures, changes in opto-electronic and magnetic behaviour and their applications in photosensing, photocatalytic, photovoltaic, magnetic, sensor, anti-microbial and medical fields are thoroughly.

2 Need for multi-functional ZnO nanomaterials

The development of novel doped ZnO having different nanostructures for multi-functional applications gained considerable attention due to their unique physicochemical properties and variable nanostructures such as thin-films, nanowires, hollow cages, nanorings, nanorods and flower like structures. The incorporation of dopants significantly transmutates the bandgap, crystalline structure, surface area, crystallite size, morphology and electronic properties of the metal oxides. In addition, these properties can also be tuned by choosing appropriate dopants and their concentration with respect to the applications and the morphology can be modified using surfactants and/or stabilizing agents.

Nanomedicine is one of the emerging fields of research in bionanotechnology because of their easy accessibility to live cells and they can be decorated with functional groups (ligands) for specific application (disease targets), which makes that the nanomedicines have potential as early diagnosis and treatment of disease of any kind [16]. Among the emerging nanomedicines, there are considerable attention have been paid for doped ZnO for application as bioimaging, biosensor, drug delivery, photodynamic therapy, magnetic resonance imaging, contrast reagents and cancer treatment [10], because of broad spectrum of anti-bacterial nature of ZnO and combined with latex used to overcome inflammation associated with cardiac implanting materials [17]. Since the ZnO is a well-known photocatalytic material, which can generate reactive oxygen species (ROS) in the biological systems, they are capable of destroying harmful microorganisms in the presence of light. On the successful doping of the metals such as Ag^{+}, Al^{3+}, Cu^{2+}, Fe^{2+}, Mn^{2+}, Mg^{2+} and Ce^{3+} in ZnO, the bandgap found be altered that promote photocatalytic efficiency of ZnO and improve anti-microbial ability of ZnO against various pathogenic Gram-positive and Gram-negative bacteria [10]. CNT and ZnO nanowire combination was used as an electrode for detecting urine albumin with 3.3 ng/mL lower detection limit [18]. For photodynamic therapy and bioimaging applications, rare earth and transition elements doped quantum dots (QDs) have explored because significant increase in the fluorescence intensity of the doped ZnO is observed as compared to the pure ZnO nanoparticles [15]. Electrospun PMMA nanofibres containing Ag NPs and ZnO nanorods showed anti-viral and anti-bacterial against pathogenic microorganisms including corona and influenza for the application as protective clothing [19].

RGB light-emitting diodes (LEDs) could be fabricated from Ce^{3+}, Tb^{3+} and Eu^{3+} doped ZnO thin films. In this study, 2% rare earth doped ZnO thin films showed narrow intense emission in red, blue and green colour, which covered whole visible region and make fulfill RGB primary colours [20]. Since ZnO is one of the versatile metal oxides (MO), it can

exhibit tunable structure and shape by means of simple synthetic methods. The doped ZnO with variable nanostructures and electronic properties can be used for the gas sensing application because of its faster sensing response and recovering time and incessant stability [21]. Therefore, the early detection of toxic and/or corrosive gas like ammonia, CO at lower detection limit (ppm/ppb) is an extremely important for working personal in pesticides, mining, pharmaceutical and fertilizers industries [22]. There are many investigations explored practicability of doped ZnO nanomaterials for ammonia, amines, sulphide, alcohol, formaldehyde and CO sensing. For instance, Cr^{3+} doped ZnO for NH_3 sensing [23], V_2O_5 doped ZnO as phenylhydrazine sensor [24], Ag^{+} doped ZnO for H_2S sensing [25], Au and Ni^{2+} doped ZnO for ethanol sensing [26, 27], Al^{3+} doped ZnO for acetone sensing [28] and Sn^{4+} doped ZnO for formaldehyde sensing applications [29, 30]. The development of gas sensor for biomarker sensing applications could be useful as non-invasive tool for early detection. Acetone is an important biomarker for diagnosing diabetes, asthma, halitosis and lung cancer. Pristine and doped ZnO having variable micro and nanostructures were used as cost-effective sensor for acetone [31].

3 Importance of nanostructures

When compared to bulk materials, the nanomaterials have higher surface to volume ratio and tailor-made nanostructures that are essential criteria for the fabrication of any sensing or catalytic devices [32]. Barium-doped ZnO nanodisks having 20–30 nm diameter with optical bandgap 3.04 eV were synthesized using sonochemical method [33]. In an investigation, the flower or coral like hierarchical nanostructure of ZnO/C-$ZnFe_2O_4$ (Z/C-ZFO) is obtained using two step hydrothermal-template assisted synthesis and morphological changes are revealed by SEM. The flower like unique nanostructure of Z/C-ZFO demonstrated significant improvement in the photocatalytic properties as compared to ZnO [34]. The nanomaterial with flower, coral, rod and wire like nanostructures showed enhanced photocatalytic and sensing properties due to their larger surface to volume ratio.

There is a continuous quest in the development of novel nanostructured materials to enhance gas sensing performance with rapid response and recovery time at ppb level of the gas, which are efficient materials as compared to bulk materials. The enhancement in physicochemical properties of nanostructured materials ensued due to large surface area, smaller size, tunable shape and structure, and consistent chemical composition [35]. For instance, vertically aligned ZnO-based nanorods with tunable growth flaunted as an excellent material for solar water splitting reactions [36]. Co-doped ZnO nanorods functionalized with metal-organic framework used as a photoanode for visible light induced waster splitting reaction [37]. Array of ZnO microrods with controllable growth synthesised using hydrothermal process showed high sensitivity photodetector [38]. HfO_2-doped ZnO nanosheet showed photodetection response from visible to near IR (1200 nm) range [39], whereas Al-doped ZnO nanosheet has been tested for pH sensor with 2–12 pH range and the sensor showed 0.3 s response time for detection [40]. The heterojunction fabricated from the nanocomposites of ZnO nanorods and K-doped nanosheets of g-C_3N_4 have been explored for photocatalytic degradation of tetracycline [41]. Controllable three-dimensional ZnO honeycomb structure synthesised by coating on carbon nanospheres under hydrothermal conditions. The growth of honeycomb structures can be controlled by optimizing the synthesis temperature and nanocarbon to zinc source molar ratio [42]. In 90 min of contact time, the honeycomb structured ZnO (Fig. 2a) showed more than 90% photocatalytic degradation of methylene blue and in contrast micro-sized ZnO achieved only 40% degradation of the same pollutant (Fig. 2b).

By adopting suitable template materials and conditions such as temperature, template to zinc source molar ratio, the growth of nanostructures controlled for diverse functional materials and under the controlled conditions, ZnO could be grown in bulk, thin film, nanowires, nanobelts, core shell, hollow cages, flower, honeycombed structure, and other morphologies. Ag-doped polyurethane templated ZnO nanowires with uniform size have been obtained by UV curable nanoimprinting lithography [43]. By using optimised combination of L-Tartaric acid (L-TA) and ethanol amine (EA), Ag-doped ZnO hollow cages synthesised for the photocatalytic degradation of methylene blue [44]. The accretion in photocatalytic degradation of methyl orange is observed for core shell Ag-doped ZnO than pristine ZnO and P-25 [45]. The ZnO nanorods covered with Ag to achieve Ag-doped ZnO nanostructures for the enhancement of photophysical and photocatalytic properties [46]. The hydrothermal synthesis of SnO and ZnO nanocomposites templated by ethylenediamine resulted in hierarchical 1D and 2D nanorod structures and showed 9 times enhancement in photocatalytic degradation of methylene blue [47]. The nanocomposite of flower like graphene with ZnO was explored for the photocatalytic hydrogen generation [48]. Similarly, Au/CdS core shell nanorods ZnO with flower like nanostructure were found to be 22.5 times higher production of H_2 than pure ZnO [49]. The nanocomposites conducting polymer, PANI with flower like ZnO showed enhanced photocurrent density than pure ZnO [50].

4 Modification of electronic properties of ZnO

For more than three decades, ZnO is a well-known n-type semiconductor having natural bandgap of 3.37 eV. With respect to the nanostructures, ZnO nanoparticles have expected

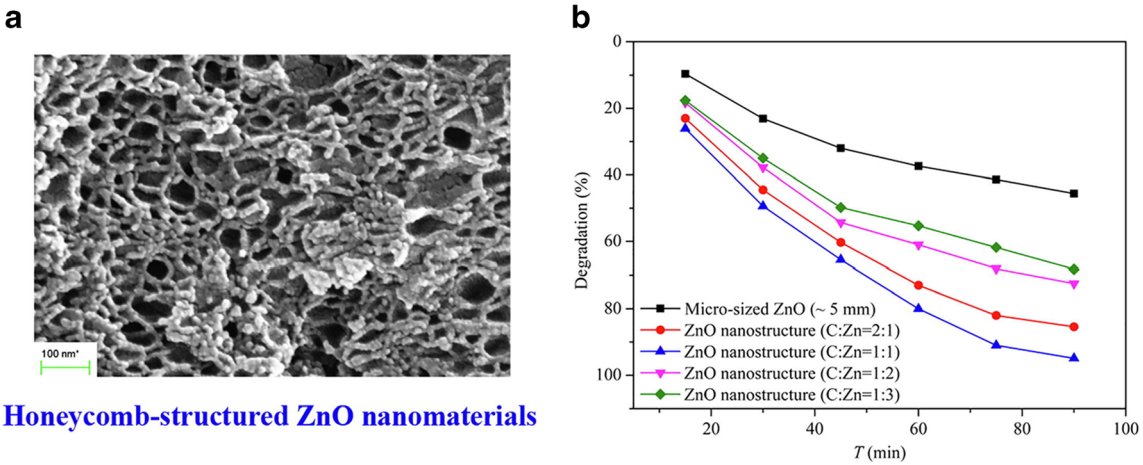

Fig. 2 (**a**) ZnO honeycomb structure; (**b**) Degradation of methylene blue (adopted with permission from [42])

to show the bandgap in the range of 3.40–3.10 eV. Electrochemical, photophysical, magnetic and sensing properties count on n-type or p-type conductivity of ZnO. Furthermore, the crystallite size, and nature and concentration of dopants are responsible for narrowing or widening of ZnO bandgap. Using simple coprecipitation or hydrothermal synthesis, dopants such as C, N, S, alkaline, alkaline earth, transition and rare earth metals can be introduced in the ZnO lattices by replacing Zn^{2+} ions or O^{2-}. The bandgap alteration could be clearly visualized using UV-Vis absorption spectroscopy and Tauc plot. Among VA elements, N-doped ZnO showed p-type conduction and improve acceptor level of ZnO [12]. As compared to N and C-doping, S-doping reduced the bandgap up to 2.52 eV [13]. Both XRD and UV-Vis studies observed that S-doping affects crystallite size as well as absorption spectra of ZnO. Most of the reports stated that S-doping resulted in red shift in absorption pattern and reduce the optical bandgap.

The crystalline structure of ZnO exhibits hexagonal close packed *(hcp)* structure with Zn and O lattices. Both Zn^{2+} and O^{2-} were surrounded by four O^{2-} and Zn^{2+} respectively in a tetrahedral geometry (Figure 3). Most studies have reported that p-type conducting properties could be introduced by substituting in the place of oxygen using N or S. In contrast, n-type conducting properties could be obtained by doping with metals, which occupy in the interstitial space or in the place of Zn^{2+} in lattice [14].

There are number of reviews on the bandgap modified metal doped ZnO are available for the application as nanomedicine, luminescence QDs, magnetic and photocatalytic applications [5, 9, 10, 14, 15, 51, 52].

5 Effect of bandgap modification

Due to poor visible light absorption and larger bandgap of pure ZnO, it cannot be directly utilized for visible light photocatalysis, magnetic and sensor applications. However, the doping enhances the application versatility of zinc oxide nanostructures. The natural bandgap of ZnO can be tuned to convert it as an interesting material for magnetic and optical applications. For instance, ZnO doped with Co^{3+} explored for its spintronics applications [53]. Similarly, doping of ZnO using 5 mol% of Cd^{2+} lowered the bandgap by lowering the level of conduction band [54]. Because of the narrowed bandgap, sulphur and nitrogen doped ZnO applied as visible light photocatalyst for the degradation of organic pollutants under solar light [13, 55]. Rare-earth metals such as Eu^{2+}, Er^{2+}, Tb^{2+}, Yb^{2+}, Ho^{2+} and La^{2+} doped ZnO QDs exhibited excellent photoluminescence behaviour with very marginal change in the UV-Vis absorption pattern [56]. In the case of QDs, the natural band gap of ZnO increased while decreasing the particle size due to quantum confinement effect.

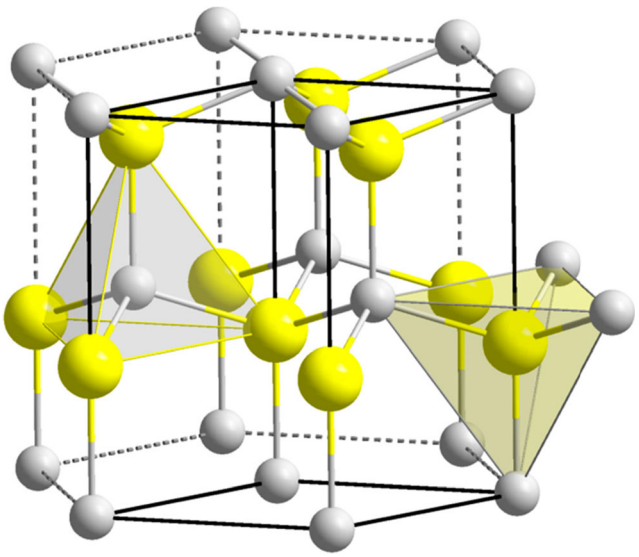

Fig. 3 Unit cell representation of Wurzite crystal. Yellow – Zn^{2+}, Grey – O^{2-} ions (Adopted from Available online: https://commons.wikimedia.org/wiki/File:Wurtzite_polyhedra.png (accessed on 02nd April 2021)

Bandgap modification affects the sensing behaviour of doped ZnO nanoparticles due to increasing n-type conducting property. Especially, the metals doped ZnO explored for sensing humidity, ammonia, ethanol, acetone, formaldehyde and amines. For instance, the nanocomposite of V_2O_5 having typical bandgap of 2.52 eV is doped with ZnO (typical bandgap 3.37 eV) and fabricated into thin film showed phenylhydrazine sensing due to increased electrical conductivity response when compared with pure V_2O_5 [24]. IVA metal Sn^{4+} doped ZnO showed increase in electrical conductivity is observed from measurement of the resistivity values and showed improved formaldehyde sensing as compared to undoped ZnO [29, 30]. Three and 5 mol% Cr^{3+} doping in ZnO reduced the bandgap from 3.22 to 3.19 and 3.18 eV respectively as calculated from Tauc relationship. Subsequently, 5 mol% Cr^{3+} doped ZnO showed more NH_3 sensing capability [23]. Photo responsiveness of ZnO increased by doping of 6wt% Nd^{2+}, which resulted in decreasing the optical bandgap from 3.31 to 3.18 eV with increase in crystallite size from 35 to 40 nm [57]. Among the 4f metals, 1, 5 and 10 mol% La doped ZnO showed marginal variation in optical bandgap as 3.30, 3.28 and 3.30 eV respectively for 1, 5 and 10 mol% of La dopant with crystallite size of 26.61, 19.61 and 20.12 nm [58]. In another study, La doped ZnO is used for the degradation of monocrotaphos and it showed better catalytic activity than pure ZnO [59]. The bandgap modification of ZnO nanoparticles using Mn^{2+} as dopant by using simple coprecipitation technique showed increase in the bandgap. SEM morphological studies showed particle size gradually increased from 150 to 509 nm, while increasing Mn^{2+} concentration from 3 to 10 mol%. In addition to the dopant concentration, the crystallite size has a major contribution for the bandgap modification. In contrast, it was blue shifted in the absorption spectra to the lower wavelength with respect to increasing of Mn^{2+} dopant concentration. Subsequently, the optical bandgap increased from 3.35 to 3.42 eV for 3 and 20 mol% Mn doping, while pure ZnO was having 3.31 eV. The modification of electronic structure of ZnO nanoparticles could be due to lattice substitution in the place of Zn^{2+} by Mn^{2+} dopant [60, 61]. Three mol% Ag doping created defects more interstitially occupied in ZnO lattice, which enhanced NO_2 gas sensing nature [62]. There are many studies in which change in bandgap upon doping with various metals have been discussed in the applications section of this review.

6 Bandgap modification using metals

ZnO is one of the significant metal oxides owing to unique physical properties, which include a large exciton binding energy of 60 meV with a bandgap of 3.37 eV [63]. It has triggered a huge interest among scientists and used in a diverse application, including sensors, optoelectronics, pharmaceuticals, and so on [64]. The optical bandgap of ZnO can be adjusted either by substitutional doping or minimizing the crystallites size. Substitutional doping can be achieved by a chemical reaction that drives the dopant element to be incorporated into the compound crystal structure. It would be possible to produce pure and single-phase materials that are isostructural to the starting compound [65]. These emerging compounds will have unique properties that will be beneficial in potential applications [66]. Though numerous works published based on pristine ZnO and doped ZnO-based materials, still there are several unsolved issues on this aspect. The optical bandgap is a well-known physical property of materials that influences their electrical behaviour [67]. The phenomenon of bandgap changes in ZnO and doped ZnO nanostructures is still poorly understood. This work attempt to explain the underlying causes behind the bandgap modification. From the perspective of crystal structure, valence bands and composition of the compounds, the mechanisms, causes, and explanations are investigated. For instance, there are no specific reasons for the mechanisms of bandgap widening in ZnO nanostructured beyond the vacancy occurrence, as some researchers have speculated but without experimental evidence.

6.1 IIIA metals (Al and In)

Metal-doped ZnO thin films with a crystalline structure in the (002) plane have been extensively studied for applications, such as transparent conducting electrode materials for solar cells, electroluminescence displays, and other electronic devices. Among the various metals (Al, Ga, In), aluminium-doped ZnO (Al-ZnO) thin film is a particularly appealing material due to its excellent properties, including good resistance to hydrogen plasma damage, increased thermal stability, and low fabrication cost [68]. As a result, a variety of fabrication techniques have been adapted to deposit Al-ZnO thin films, including magnetron sputtering, pulsed laser deposition, chemical vapour deposition, electrochemical deposition, sol–gel method, hydro- and solvothermal method and spray pyrolysis [69]. Ramírez et al. focused on the electrodeposition of Al on ZnO where bandgap value increased with increasing Al doping content [70]. According to Das et al., the bandgap of Al-ZnO is determined by the electron concentration [71]. Wang et al. reported that low-temperature ionised impurity scattering is responsible for Al-ZnO carrier mobility [72]. Hyun et al. mentioned the UV absorption edge of Al-ZnO is slightly blue-shifted with Al content addition, implying that the optical bandgap is broadening [73]. Ahmad et al. studied the effects of Al doping concentrations on ZnO lattice where light absorption increased to a maximum of 402 nm. On the other hand, the bandgap energies decreased from 3.21 to 3.12 eV as the Al^{3+} content raised from 0.0 to 6.0 mol % which attributed to band-edge bending while doping [74].

Lee et al. indicated the transmittance of Al-ZnO thin films increased slightly compared to undoped ZnO, which is due to decreased light scattering from smaller grain sizes, as confirmed by XRD results [73]. Maldonado et al. used a statistical model to quantify the bandgap. The bandgap diameter observed as a differential between the highest occupied molecular orbital (HOMO) and the lowest unoccupied molecular orbital (LUMO) is around 4.1 eV, which is similar to the experimentally established magnitude of 3.37 eV [75].

It is significant to mention that ZnO electrical properties are inadequate to satisfy the growing demand for high-performance semiconductor devices [76]. Though, Tin-doped indium oxide (ITO) is used widely as transparent conducting oxides where indium is the major component, and it is very expensive. Therefore, to overcome the challenge faced by ITO and ZnO, doping trace amounts of group III elements (Ga, Al, and In) onto ZnO can alternatively improve their optoelectrical properties [77]. Out of all the dopants, indium (In) is the most effective element for enhancing the ZnO film conductivity [78]. The applicability of ZnO thin films as sensors, transparent electrodes or optoelectronic devices is determined by structural defects in the ZnO lattice, which are dependent on the presence and concentration of dopants [79]. Numerous literatures focused on Indium-doped ZnO (In-ZnO) thin films as In facilitates preferential (101) orientation in ZnO and decreases grain size. According to Prasad et al. the ammonia sensing properties and optical properties of ZnO thin films decreased as the concentration of In in the films increased [80]. Dintle et al. were able to adjust the crystallographic orientations, microstructure, optical and electrical properties of ZnO thin films by varying the In doping material [81]. Winkler et al. developed spray pyrolysis-prepared highly transparent and conductive In-ZnO thin films which were ideal and can be used in photovoltaic and optoelectronic devices [82]. Bharath et al. claim that gas sensing and electrical properties are improved with an In doping concentration of about 3 at. % [83]. The higher optical bandgap variation was found by Ahn and Kim et al [84]. The optical bandgap energy of pristine ZnO nanoparticle suspensions was 3.28 eV and decreases to 3.26 eV after varying In doping concentration, according to Sahoo et al [85]. Further, Bae et al. mentioned the bandgap values of In-ZnO thin films reduced from 3.29 to 3.25 eV as the In doping increased with the bandgap shifted towards the red region [86].

6.2 IVA metals (Sn and Pb)

Among the group IVA elements, Tin-doped ZnO (Sn-ZnO) has emerged as a promising and fascinating component for high-performance photodetectors due to its high carrier mobility, high absorption coefficient and relatively narrow bandgap [87], extending Sn-ZnO application further to solar cells as a transparent conducting electrode. To establish the electrical properties of ZnO thin films by RF magnetron sputtering, the content of group IV impurity incorporation to the ZnO target was controlled [88]. Sn-ZnO films with a 1 wt % doping content had a higher resistivity than the undoped film. This is due to increasing the Sn content decreased hall mobility while marginally increasing carrier concentration [89]. As a result of the yellow colouration of Sn-ZnO films, there was significant visible region absorption as well as an increase in UV emission (redshift) [90]. Benelmadjat et al. mentioned the optical bandgap of ZnO films decreases as Sn doping content increases which ascribed to the band shrinkage effect as carrier concentration increases [91], while Saha et al. observed the optical bandgap broadening for Sn-doped samples from 3.08 (pristine ZnO) to 3.17 eV. However, Sn incorporation of ZnO nanowires has compromised optical transmission properties due to the maximum absorbance [92]. Similarly, Ganesh et al. revealed that the optical bandgap broadens with increasing Sn doping concentration on ZnO thin films [93], while Tan et al. found the optical bandgap of ZnO thin films by metal-organic chemical vapour deposition has blue-shifted [94]. Liu et al. investigated with Sn-ZnO where UV emission broadens towards higher wavelengths which may be due to a reduction in the bandgap [95].

Numerous researches perform on metal doping in ZnO. However, high-quality crystalline with outstanding electrical and optical properties in doped ZnO nanostructures is still a concern. Many groups focused on lead-doping in ZnO (Pb-ZnO) due to their larger ionic radius of Pb^{2+} (1.19 Å) than Zn^{2+} (0.74 Å) [96, 97]. Despite, Zn is more active than Pb in the chemical reaction. Pb can quickly be replaced by Zn in vapour reactions, resulting in Pb-doped ZnO. By adjusting the lead (Pb) stoichiometry ratio, Pb is a strong dopant for lowering the bandgap of ZnO [96]. Yousefi et al. observed the optical bandgap values obtained for x = 0, 2, 5, 8, and 10 wt % Pb doping content are 3.40, 3.38, 3.36, 3.35, and 3.30 eV, respectively [98]. The bandgap decreases as the amount of Pb dopant increases due to the creation of new energy levels between the valence band and the conduction band owing to the B-M effect. In contrast, Boumaiza et al. noticed that the ZnO bandgap is 3.19 eV, but that as the Pb doping concentration increased to 5 and 10%, the bandgap also tuned to 3.26 and 3.3 eV, respectively, due to the quantum confinement effect [99]. Ali et al. found that the ZnO energy bandgap is 3.21 eV and slightly increased to 3.23 eV after Pb doping which can be ascribed to the increased carrier concentration [100]. Furthermore, according to Boumaiza et al., an increase in Pb concentration causes the bandgap to broaden as the crystallite size reduces [99]. Kannadasan et al. also observed the blue-shift on the doping of Pb to ZnO [101]. Interestingly, Inigo et al investigated the properties of a Pb-ZnO thin film where they observed that Pb doping modify the optical and structural properties of ZnO. Furthermore, as the doping

concentration increases, the transmittance improved in the near-infrared region (800–1100 cm^{-1}) [102]. Similarly, Sathya et al. mentioned for Pb doping (x = 0, 2, 5, 8, and 10 wt. %), the bandgap value narrowed (3.40, 3.38, 3.36, 3.35, and 3.30 eV) [103].

6.3 VA metals (Sb and Bi)

Recently, many researchers have focused on Antimony-doped ZnO (Sb-ZnO) as the Sb doping improves the transparency and also tune the bandgap towards the visible region. However, there are only a limited Sb-doped ZnO reports in the literature [104]. Aoki et al. developed an Sb-ZnO film using an excimer laser doping technique where Sb accumulated on the intrinsic ZnO film. Furthermore, an excimer laser-driven the Sb impurities into the ZnO film. The acceptor energy level of the Sb dopant is around 0.2 eV above the valence band, based on temperature-dependent PL analysis [105]. According to Yung et al, the transmittance values decrease as the Sb dopant concentration increases to 3%, resulting in a redshift of the transmittance edge in the UV region [106]. Pure ZnO film has an estimated bandgap of 3.26 eV, which increases to 3.30, 3.31, and 3.32 with 3, 5, and 10% Sb, respectively. This is due to the high carrier material, which shifted the optical absorption edge to a lower energy state [107]. The bandgap energy observed to be 3.26 eV for pristine ZnO while for 1, 2, and 3% Sb doping is 3.05, 2.92, and 3.09 eV which attributed to the low band tailing effect and defect-like interstitial zinc atoms [108]. The slight variation in bandgap energy is due to stoichiometric variations caused by different doping concentrations [109]. Additionally, Jagadhesan et al. perceived pure ZnO and Sb (0.05 % and 0.075 %) doped ZnO and estimated the bandgap to be 3.75, 3.83 and 3.81 eV, respectively [110]. However, Baek et al. mentioned that the bandgap values obtained for Sb-ZnO decreased from 3.35 eV for pristine ZnO to 3.15 eV for Sb-ZnO. The intensity of the absorption edge increases with Sb doping because the electron-hole separation rate on the ZnO surface improves [111]. According to Benelmadjat, the bandgap increases as Sb doping concentration increases from 2 % (3.41 eV) to 7 % (3.51 eV). Incorporating Sb into ZnO thin films increases stress by modifying cell parameters as Oxygen atom is substituted, theoretically creating ZnO crystallite fractures since the radius of the Sb ion is greater than that of the O_2 [112]. According to Mandalapu et al, Sb mainly occupies zinc lattice positions and acts as a donor. At higher Sb content, it is most typically on oxygen lattice positions, resulting in acceptor behaviour. The defects of these predicted p-type dopants have complicated chemistry [113].

Bismuth (Bi) is a Group VA element that is abundant in natural sources, has high chemical stability in its trivalent form and is less toxic than Pb^{2+} and Sn^{2+} [114]. The electronegativity, ionic radius, and electronic structure of the Bi ion are similar to those of Pb^{2+}. However, during the Bi ion incorporation into the ZnO lattice, the *sp–d* exchange interaction between the localised d-electrons and band electrons of the Bi ions occurs [115]. Moreover, the electron transfer from the valence band to the conduction band increased the absorbance after 365 nm, which ascribed to the increase in absorbance (O2p-Zn3d). By incorporating Bi into ZnO (Bi-ZnO), the absorbance edge is blue-shifted [116]. The bandgap of the pristine ZnO and Bi-ZnO are 3.23 and 3.28 eV, respectively [117]. Zahirullah et al. stated that as the concentration of Bi increases from 0 to 5%, the optical absorption edge red-shifted [118]. According to Karthikeyan et al., Bi doping on ZnO increases the bandgap from 3.19 to 3.24 eV which can be described by the B-M effect. Since the Pauli principle prohibits doubly occupied states and optical transitions are vertical, valence electrons must be excited with additional energy [119]. Similarly, Keskenler et al. mentioned the varied bandgap ranging 3.28, 3.25, 3.31, 3.31 and 3.17 eV for Bi-ZnO. The optical bandgap fluctuates owing to the broadening of valence band and conduction bands caused by interactions between Bi *s, p* and *d* electrons and host atoms [120]. According to Jamal et al. the optical bandgaps for pristine, 1, 3, and 5% Bi- ZnO nanowires are 3.35, 3.26, 3.30, and 3.28 eV, respectively. Bi-doping reduces the optical bandgap of ZnO nanowires by producing permissible energy states within the bandgap, resulting in a redshift [121].

6.4 IB group metals (Cu, Ag and Au)

Among various dopants, copper-doped ZnO (Cu-ZnO) nanostructures are extremely useful in a variety of applications due to the substantial improvement in physical and chemical properties [122]. Recently, Cu-ZnO nanoparticles with a bandgap of 3.4 eV were synthesised by the precipitation method, signifying that the copper (Cu) dopant concentration plays a significant role in enhancing their PL properties [123]. Chakraborty et al. found that Cu-ZnO (Cu doping concentration 5–10 %) has a lower bandgap value (3.07 eV) compared to pristine ZnO (3.21 eV) and caused in a blue absorption edge transition as the Cu doping diminishes the electron-hole pair recombination [124]. Kayani et al. confirmed that as the Cu doping ratio increases from 2 to 10 wt%, the crystallite size of the Cu-ZnO thin film increased [125]. Besides, Cu doping causes the bandgap in Cu-ZnO thin films to decrease insignificantly. Ouidette et al. mentioned that the Cu dopant uniformly substituted Zn sites and crystallite sizes of 32–38 nm for ZnO and Cu-ZnO nanoparticles [126]. As the impurity band and the conduction band were merging, the optical absorption spectra revealed a red absorption edge. The scattering of excitation radiation by the non-radiative recombination mechanism and surface-adsorbed Cu dopant atoms causes the visible PL intensity to decrease as the Cu content increases. According to Fang et al., Cu^{2+} doping did not result in the

secondary phase formation, whereas it significantly decreased the particle size [127]. Additionally, the PL intensity (excitation wavelength ~ 325 nm) reduced with increasing Cu doping content. Das et al. mentioned that the *sp-d* exchange interaction between the localised d electrons of Cu^{2+} ions and ZnO band electrons causes the bandgap of ZnO to decrease with Cu doping [128]. Zheng et al. found the p-type Cu-ZnO since its impurity level of 0.1 % Cu are higher than the Fermi level [129]. Zhanhong et al. observed the conduction band shifted downwards as Cu concentration increased, the bandgap of $Zn_{1-x}Cu_xO$ decreased [125]. On the other hand, Aravapalli et al. observed the maximum absorbance for 0.3 % Cu-ZnO nanoparticles, showing bandgap reduction as Cu doping concentration increases [130].

Among various transition metals, Gold (Au) has received a lot of recognition as a noble metal. The formation energies of Au ions with positive univalence at Zn sites of ZnO are much lower than at interstitial sites, according to first-principle calculations, so substitutional doping of Au element in ZnO will significantly prevent self-compensation and is considered an efficient p-type doping procedure [131]. Though, Au has 3 types of valence and only univalent Au ion occupying the Zn site of ZnO serves as chemical state regulation, an acceptor and substitutional doping are critical for obtaining p-type Gold-doped ZnO (Au-ZnO) [132]. Recently, Au-ZnO thin films and nano-powders have also been studied due to their fascinating photocatalytic and sensing properties [133]. The bandgap of Au-ZnO is smaller than that of pristine ZnO, indicating that Au-ZnO is more electrically active than pristine ZnO since more free electrons are available as donors [134]. According to Ouarez et al., the bandgap value increases to 3.298, 3.307, 3.315, and 3.325 eV as Au concentration in ZnO increases to 0, 10, 20, and 30 at% which attributed to the B-M effect as confirmed via the increase of the carrier concentration [135]. Rahman et al. recently informed the widening of the bandgap with increasing Au material in Au-ZnO films [136]. Deshwal et al mentioned with Au nanoparticles doping on ZnO, the energy bandgap decreased from 4.01 (pristine ZnO) to 3.7 eV (Au-ZnO) [134]. This may be attributed to the presence of more dopant atoms near the surface of ZnO, which would accumulate oxygen vacancies and serve as donors to enhance the thin-film electron concentration [94]. Hence, the Schottky barrier height will be lowered and the electron tunnelling mechanism will prevail in producing ohmic characteristics of ZnO with Au contacts leading to a lower bandgap for the ZnO thin film [137]. Wang et al. observed the optical bandgap of the Au-ZnO is smaller than pristine ZnO, which attributes the Au dopant effect [138]. The strong p-d coupling between Au and O happens when the Au atom occupies the Zn site, increasing the O2p level and narrowing the bandgap [132].

ZnO nanostructures possess poor optical properties and a tendency for point defects such as oxygen vacancies; thus, ZnO cannot be used actively in industries [139]. Hence, noble metal doping of ZnO is desirable. When compared to pure ZnO nanoparticles, several studies show that Au-ZnO and Pt-ZnO exhibit high photocatalytic activity. However, Silver (Ag) is comparatively inexpensive than Pt and Au, so it could be ideal for the industrial application of Ag-doped ZnO (Ag-ZnO) [140]. The Surface Plasmon Resonance (SPR) occurs near the surface of Ag-coated particles, which improves optical absorption and inhibits the electron-hole pair recombination [141]. Deepika et al. observed the red absorption edge which attributed to bandgap narrowing of ZnO as the Ag concentration increases [142]. Similarly, Ahmad et al. informed the bandgap narrowing in Ag-ZnO films with increasing Ag content [143]. Ruby et al. mentioned with increasing temperature from 300 to 800 °C, the bandgap values of pristine and Au-ZnO decrease [144]. The difference in absorption edges is triggered by the incorporation of Ag nanoparticles on the ZnO surface, which causes an electron to transition from the valence band to the conduction band through the bandgap [145]. Rahini et al. mentioned the bandgap reduction in Au-ZnO can be attributed to higher electrons excitation resulting in an electron transfer from the Ag conduction band to the ZnO lattice, encapsulated content, and the ionic radii difference between two metals [141]. On the other hand, Saboor et al. mentioned the absorption spectra of Ag-ZnO nanorods exhibited blue-shifts centred at 375 and 368.5 nm when the Ag dopant concentration was raised to 5% and 7%, respectively which is ascribed to the intense chemical interaction between Ag and Zn surface oxides, as well as the quantum size effect [146]. The B-M effect explained the blue-shift in the optical absorption spectra at dopant concentrations greater than 3% as it causes an increase in charge carrier concentration [147].

6.5 IIB (Cd and Hg)

Among various dopants, currently, the doping of cadmium (Cd) in ZnO has received great attention as by doping ZnO with Cd, its absorption edge can be red-shifted. Furthermore, the synthesized materials will maintain the ZnO wurtzite hexagonal phase owing to the almost identical ionic radius of Cd^{2+} (0.60 Å) and Zn^{2+} (0.74 Å) [148]. Mondal et al. discovered that as the Cd-doping level increases, the fundamental absorption edge declines, explaining the significant difference in bandgap values between CdO and ZnO [149]. The narrowing bandgap energy, according to Jianfeng et al., is caused by the presence of Cd impurities in the ZnO, which cause the development of recombination centres with low emission energy. Electronic transitions to impurity levels are thought to be responsible for the change in absorption [150]. Similarly, Ghoderao et al. pointed out that a redshift in the absorption edge showed a decline in bandgap value as doping concentration increased. The bandgap value changes based on a variety

of factors such as carrier concentration, grain size, lattice strain, and so on. The formation of energy levels within the conduction band and valence band can also be responsible for the reduction in bandgap [151]. Furthermore, Cd doping in ZnO resulted in bandgap reductions, resulting in luminescence tuning from ultraviolet to visible [152]. According to Mitrushchenkov et al. theoretical study, the addition of mercury (Hg) to ZnO nanowires increases the piezoelectric properties dramatically [153]. While Saravanan et al. mentioned the bandgaps of pristine ZnO (3.2 eV) in the blue region and Hg-doped ZnO (3.11 eV) is extended into the red region [154]. They later reported in another report that the bandgap of Hg doped ZnO narrowed from 3.2 eV (pristine ZnO) to 2.8 eV with increasing Hg doping content (0.1, 0.3, and 0.5%). As the bandgap is narrower, electron transfer from the valence band to the conduction band is easily facilitated, implying that Hg doped ZnO nanorods would have a higher photocatalytic efficiency than ZnO nanorods [155].

6.6 Other transition elements

To enhance the electrical and optical properties of ZnO, various 3d transition metals (3d-TM) such as Fe, Ni, Co, Ti, Cr, V, Cu, and Mn have been tried as dopants. Because of its ferromagnetic nature at room temperature, Co, Cu, V, Cr, Mn, and Ni are considered as appropriate dopants of ZnO for spintronic devices and magneto-optical communication devices, while the other 3d-TM dopants, Fe, Co, and Ti, are recognized as efficient ZnO dopants for optoelectronic device fabrication and optical communication [156, 157]. The efficiency of a dopant element is determined by its ionic radius between Be and ZnO and its electronegativity. According to Bhat et al., the optical bandgap for pristine ZnO is 3.22 eV, but it decreases to 3.11 eV with increasing Ni doping content, indicating that the bandgap values of ZnO are dependent on the doping % and thus it can be tuned by adjusting their stoichiometries constituent. Similar behaviour for ZnO with manganese and cobalt has also been reported [158]. Remarkably, EPR studies reveal that manganese ions are incorporated in (T= 425 and 500 °C) or at surfaces (T > 500 °C) of ZnO nanoparticles, depending on annealing temperature [159]. Likewise, Amjid et al. predicted the bandgap energy to be decreased with increasing chromium doping concentration [160]. Joshi et al. discovered that vanadium-doped ZnO has a lower bandgap than pristine ZnO, which they attribute to the alloying effect between ZnO and V_2O_5 [161]. On the other hand, Ozkan et al. claimed that the optical transmittance of nickel-doped ZnO thin films was greater than 90%, though this value appears to decrease marginally due to Ni doping. Furthermore, as Ni doping increased, the optical bandgap decreased at first, then increased marginally [162]. As per Talaat et al., the B-M effect causes a blue-shift in the bandgap of Cobalt-doped ZnO as an increase in carrier concentration where Fermi level merges with conduction band and block the low-energy transitions [163]. Moreover, a minor shift toward higher magnetic fields with increased doping concentration of the Cobalt-doped ZnO NPs clearly demonstrates that the doping atoms have an influence and have an impact upon the local ferromagnetic interaction disorder [164]. However, Sung et al. found that optical transparency of zirconium (Zr)-doped ZnO thin films was greater than 90%, while the optical bandgap increased (3.25 to 5.1 eV) with Zr content [165]. Srinivasulu et al. revealed the higher optical transmittance for lower iron-doped films with a significantly increased bandgap than for pristine and heavily doped films [166]. In contrary to the literature, Aslan et al. observed the bandgap of Titanium-doped ZnO observed with no significant change due to a decrease in carrier concentration [167]. The carrier density of a semiconductor varies with doping atoms and defects in the structure.

6.7 IA and IIA metals (Li and Be)

Group-IA elements may be more suited for p-type doping which may lead to stabilization since they provide lower energy levels with depth. Amongst group-I elements, Li has the least ionic radius (0.90 Å) which is similar to Zn (0.74 Å), and this is a substantial factor in obtaining high optical efficiency in p-type ZnO [166, 168]. According to Lander, Li may function both as a donor and as an acceptor in ZnO. When Li substitutes at a Zn site, the acceptor behaviour is observed, and when Li appears at an interstitial site, the donor behaviour is observed [169]. The optical bandgap is observed to marginally increase after Li doping (from 3.25 to 3.28 eV). This bandgap widening may be ascribed to the Burstein-Moss (B-M) effect, which indicates that certain states near the oxides conduction band have been populated; this implies n-type doping of ZnO during Li intercalation, as doping with acceptors (p-type) has been shown to result in a bandgap reduction of ZnO [170]. Since Li^+ ions substituting Zn^{2+} ions are assumed to be acceptors, their functionality as n-type dopants means that they most likely occupy interstitial sites. It is worth noting that the transmittance of ZnO is unaffected by Li doping and stays strong enough to cause the majority of the illuminated light to pass through to the photoactive layer [171]. Doped thin films, on the other hand, have a bandgap narrowing of around 0.02 eV as opposed to undoped ZnO thin films; this low reduction may be interpreted by grain size growth [172]. Despite the reduction in grain size, a bandgap narrowing is observed for $x = 5\%$; this may be due to local electric fields caused by disorder, impurity, or other defects that impact the band tails along the band edge [173]. The bandgap of ZnO widens when $x > 5\%$ which is extremely prone to minor changes in grain boundary orientation, carrier concentration, and film stress [174, 175]. Likewise, the bandgap widens with Li doping ($x < 50\%$) on ZnO films

which may be explained by (1) B-M effect and (2) the shallow donor Zn sublevels transform to deep-sublevels below the conduction band [176]. Controversy, there is an obvious bandgap narrowing for heavy Li-doped thin films ($x > 50\%$), this may largely a consequence of conduction-band renormalization [172].

The element Beryllium (Be) typically emerges as a potential candidate for photodetectors and short-wavelength light-emitting devices due to ZnO bandgap modification. There are few considerations for Be-doped ZnO which follows, (1) both ZnO and BeO possess stable hexagonal wurtzite structure, (2) Be solubility in ZnO varies with composition range, and there is no phase separation between ZnO and BeO, (3) BeO has a large bandgap about 10.6 eV which tune bandgap over a broad range of 3.4 to 10.6 eV, (4) combining Be and ZnO, the $Be_xZn_{1x}O$ alloy can be easily produced [177–179]. Several experimental studies have been published to reveal different properties of $Be_xZn_{1x}O$ films, as well as first-principle calculations to examine the Be concentration effect on $Be_xZn_{1x}O$ films properties [180]. Because of its minimal ionic radius (0.35 Å), Be has a better possibility of occupying the interstitial positions of the ZnO lattice [181]. Remarkably, there is a disparity between experimental and determined results, i.e. the bandgap of $Be_xZn_{1x}O$ increases with increasing Be concentration, and the lattice constant of $Be_xZn_{1x}O$ observes a related pattern [182]. Calculations also demonstrate that replacing Zn atoms with Be increases the bandgap of ZnBeO phases, while interstitial Be atoms decreases the bandgap, and that these bandgap changes are primarily due to increased metallic and covalent bonding as a result of Be doping [183]. According to Ye et al., the quantity of Be atoms incorporated into the ZnO lattice reduces in $Be_{0.1}Zn_{0.9}O$, resulting in a narrower bandgap than $Be_{0.06}Zn_{0.94}O$ [184]. The enhancement of N doping efficiency and the reduction in the ionisation energy of acceptor N_O are two major benefits of the Be atom integration, based on Chen et al. [185]. While the bandgap seems to decrease as the deposition temperature rises, it should be remembered that the bandgap of Be-ZnO is still larger than that of undoped ZnO, posing a greater potential barrier to charge injection [186].

7 Bandgap modification using non-metals

Non-metal doping of ZnO has been studied extensively, which is intended to substitute for lattice oxygen atoms and thus introducing oxygen vacancies that occupy interstitial zinc atoms. In the non-metal doping case, hybridization of O 2p states of ZnO and non-metal dopant orbitals raise the valence band maximum and accordingly bandgap narrow to the UV-visible region [187]. Non-metal doping, in contrast to metal doping, is less probable to form recombination centres, extending the lifespan of charge carriers. Effective non-metal dopants must have a lower electronegativity than oxygen and an atomic radius that is similar to that of lattice O atoms [188]. ZnO doping with p-type non-metals, such as carbon (C), nitrogen (N), boron (B), phosphorous (P), Silicon (Si) and sulfur (S), leads to the intermediate energy levels formation along with extending the valence band upwards. Moreover, extrinsic doping is typically more stable compared with the intrinsic donors resulting from native defects [189]. Details of the ZnO doping process using diverse non-metals are considered to be a conceptually promising and simple strategy to enhance the ZnO properties, and the outcomes are discussed.

7.1 IIIA (B)

Among group IIIA elements, boron (B) is gaining a lot of interest these days as a potential cationic doping ZnO (B-ZnO). Because of its highest electronegativity (2.04, Pauling) and the ionic radius (0.23 Å) analogous to Zn^{2+}. Furthermore, the Lewis acid strength of B^{3+} (10.7) is significantly higher than that of Al^{3+} (3.04) [190]. As a result, boron doping can be useful for modifying the physical properties of ZnO. Tsay and Hsu et al. studied how the properties of ZnO thin films are affected by boron doping concentration [191]. According to the findings, B-ZnO thin films optical bandgap slightly shifted towards higher energies compared to pristine ZnO thin film. In B-ZnO thin films, Houng et al. noticed that the optical bandgap values varied depending on the crystalline structure owing to its grain size effect [192]. Along with the grain size effect, there is also an increase in charge carrier density by the substitution of B^{3+} in a Zn^{2+} site as a donor. Furthermore, the Urbach energy of B-ZnO thin films increases with increasing B doping concentration indicating the structural disorder and defects [193]. Vinod et al. observed a blue shift in the UV absorption edge with a higher B concentration in ZnO film, suggesting the broadening of the optical bandgap [194]. The bandgap in heavily doped semiconductors is increased due to the blocking of low-energy transfers, according to the Burstein-Moss (B-M) shift. On the other hand, Kayani et al. realized that as the B concentration increased, the bandgap of the ZnO films decreased owing to an increase in dislocation density [195]. Steinhauser et al. conveyed the optical absorption edge is affected by bandgap narrowing with increasing carrier density due to electron-electron repulsive interactions and potential screening due to the presence of several electrons [196]. According to Bhattacharjee et al., there is a blue-shift with an increase in B concentration of up to 3% then the bandgap started to reduce at 5% B concentration [197]. The carrier concentration is quite high (> 1 at. %) in B-ZnO films with high doping concentrations where the donor level relating to B impurities in the ZnO energy band eventually widens and merges with the conduction band. As a result of the merging, the ZnO bandgap narrows suddenly which rapidly shifts the optical absorption edge to the large

wavelength orientation. According to Wang et al., the B incorporation caused an improvement in the ZnO lattice constant along with a change in its internal stress [198]. Jana et al. noticed that the dopants starting substance can also be a dominant factor [199]. For instance, Tahar et al. used boron tri-i-propoxide which containing B up to 1.4 at. % resulted in the optical bandgap of ZnO thin films with no distinct deviation [200]. Alternatively, Tumbul et al. used trimethyl borate, which demonstrated a prominent influence in optical bandgap property even at a very low concentration of B (0.2 at. %) [201].

7.2 IVA (C and Si)

Carbon (C) has been extensively used as a dopant to modify the optical properties of ZnO to overcome concerns relating to the poor performance of oxide semiconductors [202]. Furthermore, substitutional doping with atoms of identical size occurs easily as it requires low energy relative to varying atomic radii. As a result, replacing oxygen (O) atoms in the ZnO matrix with C atoms have favourable thermodynamics than using other nonmetal dopants. Furthermore, the majority of the C was incorporated at the interstitial or Zn sites, or C clusters formation, rather than at the O site [203]. According to Jailes et al., the energy bandgap of a wide-band semiconductor can be reduced by doping ZnO with carbon or forming a C-ZnO composite [204]. The redshift in energy bandgaps observed by Luyolo et al. with increasing carbon dopant levels is most likely owing to the size confinement effect [205]. Similarly, the redshift absorption was observed by Zhang et al. as the powder colour changed from white (pristine ZnO) to lavender (C-ZnO) [206]. Cesano et al. predicted that C doping in the ZnO lattice can lead to the development of impurity states in the bandgap which causes redshift in the optical absorption spectrum owing to its optical transitions from the impurity states to the conduction band [207]. Therefore, the incorporation of C on the ZnO crystal lattice leads to an intermediate energy level in the bandgap which enables it to harvest visible light from the solar spectrum [208]. Cho et al. found that C-ZnO nanostructures using vitamin C absorb more visible light than pristine ZnO nanostructures [209]. According to Lavand et al., the photogenerated charge carrier separation can be promoted by transferring photoexcited electrons to nanosized C on the catalyst surface [210]. Ansari et al. examined the effects of oxygen vacancies and Zn-C on electron-hole recombination rates [211]. On the other hand, Wang et al. conveyed that the bandgap narrowing may be due to oxygen vacancies and Zn−C formation which triggers a visible light response in C-ZnO [212].

Silicon (Si) is also a well-known tetravalent dopant that is used to improve the optical and electrical properties of III–V semiconductors by occupying cation sites. Utilizing Si as a dopant material in ZnO could not only tuning its electronic properties but also improve its practicality in Si-related devices. The electronegativity of Si (1.9) and Zn (1.65) atoms, as well as their identical atomic sizes of Si (1.17 Å) and Zn (1.33 Å), reveals their similarities [213]. Therefore, Si diffuses easily into the ZnO lattice and forms a new phase (Zn_2SiO_4) particularly at high temperatures [214]. Chowdhury et al. focused on two types of defects in ZnO: (1) Zn substitution by Si and (2) O substitution by Si [215]. Furthermore, when Si is substituted for Zn in the ZnO lattice, it is predicted to behave as a two-electron donor, potentially generating higher free carrier densities at a specified doping level than the one-electron Group 13 dopants (Al, Ga, or In) [216]. Moreover, Howard et al. revealed that the Si^{4+} site in the Zn^{2+} plane serves as a point defect that leads to localized planar defects and trapping oxygen ions owing to its higher carrier density compared to nearby Zn^{2+} ions. Therefore, when opposed to trivalent dopants, transparent conducting oxides (TCOs) can be made with lower dopant concentrations [217]. When pristine ZnO thin films were doped with Si, the resistivity of the thin films decreased while the bandgap increased [218]. The increase in bandgap with doping is well established as a consequence of the B-M effect, which occurs in degenerately doped semiconductors [219]. Likewise, Kuznetsov et al. observed the B-M blue-shift of the ZnO optical bandgap transition in the UV region is caused by increasing carrier concentration [220]. Jianwei et al. mentioned the challenge still exists in controlling the content of Si-ZnO [221]. Minami et al. had previously highlighted the interest of the Si-ZnO system, showing a minimum resistivity of 3.8×10^{-4} Ωcm for Si-ZnO thin films which deposited using RF magnetron sputtering below 250 °C [222]. Clatot et al. observed the optical bandgap values as a function of the deposition substrate temperature [223].

7.3 VA (N and P)

Among non-metal dopants, nitrogen (N) (1.68 Å) has an ionic radius equal to oxygen (O) (1.38 Å), making it an excellent p-type dopant for other II–VI semiconductors. Substituting N on an O site (N:O) is one choice in ZnO (N-ZnO), but theoretical calculations indicate that the hole binding energy is about 400 meV, which is too high for significant ionisation to occur at room temperature [224]. Additionally, substituting the N to O site by leaving a Zn-vacancy behind and thus the formation of a shallow defect complex with high barrier energy [225]. Moreover, hydrogen could stabile N:O pairs by the interaction between H and N:O which act as donor-acceptor pair (DAP). These interactions could bring extremely deep acceptor levels closer to the valence band [226]. Consequently, Yu et al. found that doping ZnO with N atoms increases its light absorption in the visible range significantly [227]. Furthermore, the redshift in absorbance found by Kale et al. suggests the probability of N doping in the ZnO structure

[228]. Renu et al. noticed a slight blue-shift in the bandgap energy of N-ZnO, indicating that the prepared nanoparticles had weak quantum confinement [229]. Besides, the reduction in bandgap in N-ZnO films is most likely ascribed to the decrease in ionicity of the Zn-N band [230]. Therefore, the incorporation of an N dopant in the crystal structure of ZnO causes the bandgap to narrow, allowing it to be activated with lower-energy radiation [231]. In contrast, Rowshon et al. reported that ZnO nanocomposites have higher UV transmittances than N-ZnO nanocomposites, which attribute to the higher bandgap of ZnO than N-ZnO [232]. However, if the carrier concentration in the ZnO thin film is higher, the B-M effect appears to be responsible for the expansion of the bandgap in the ZnO thin film [233]. Subsequently, Hongchun et al. claimed that the doping process not induced a variation in the material bandgap [234]. Conversely, Chiara et al. mentioned the increase in photocatalytic activity for N-doped systems which could be ascribed to the existence of intra-bandgap states but not to a variation in the material bandgap [235].

The stable p-type-doped ZnO commercialization remains a challenge owing to its instability of dopant in ZnO along with their low doping efficiency. Among other non-metals, Phosphorus (P) has been revealed to be one of the most effective dopants for p-type doped ZnO. According to Allenic et al., phosphorus-doped ZnO (P-ZnO) thin films were found to be stable for up to 16 months in ambient conditions [236]. Thereby, stability/degradation issues of ZnO can be avoided by P doping. Conversely, the doping mechanism of P-ZnO is still debated [237]. At least two stable configurations of P exist (1) combining substitutional P (P_Z) and two zinc vacancies (V_z) which lead to complex (P_z+2V_z) formation; (2) substitutional P at oxygen sites (P_O). The efficient configuration for p-type doping was believed to be P_z+2V_z, which makes a shallow acceptor level in the bandgap, whereas P_O was assumed to induce a comparatively deep acceptor level, not participating in enough hole concentration in ZnO [238]. P_z+2V_z is accountable for the majority of the p-type conductivity found in P-ZnO, and high resistance in P-ZnO is often thought to be caused by P_O [239]. Furthermore, the bandgap of undoped ZnO decreased until it reached 0.1 % P doping, after which bandgap increased above this concentration [240]. Certainly, extracting the bandgap from the Tauc plot is perhaps not an appropriate method as the Tauc plot disregards the excitonic effect. The PL measurements were performed to resolve this issue. Many of the PL spectra have two notable peaks, as can be seen (1) the UV region is linked to the bandgap near-band-edge emission (NBE), and (2) the visible and near-infrared regimes are linked to the ZnO deep-level emission (DLE) [241]. Conversely, the origin of the DLE in ZnO is debatable, and it is believed to be caused by a combination of defects and/or vacancies. The bandgap attained by PL is 10 meV smaller than that obtained by the Tauc plot. The bandgap of undoped ZnO nanorods from PL, for example, is 3.27 eV, leading to a 379-nm emission, while the Tauc plot is 3.28 eV, owing to the Stokes shift [242]. This emission endures a bathochromic transition from 379 to 384 nm as the doping content increases from 0 to 1%. Previous studies have shown that P doping causes an emission at 384 nm, which is caused by DAP transitions [243]. As a result, the redshift in the ZnO nanorods can be due to P-induced DAP emission. On the other hand, with an increase in oxygen (O_2) flow rate, the UV peak intensity increases, and deep-level emission is suppressed [244]. Furthermore, as the O_2 flow rate increases, the UV peaks blue-shifted, while the green peaks red-shifted. The variation of the ZnO bandgap through the band tailing effect is most probably responsible for the shift in UV emission [245]. The Urbach tailing of the band-edge into the forbidden-gap region (corresponds to the absorption edge sharpness) is influenced by structural disorder, impurity and defect states, temperature, and carrier concentration [246]. With a higher O_2 flow rate, there are fewer defects in ZnO and its crystal quality improves, weakening the band tailing effect and changing the tail width; hence, the bandgap of ZnO increases, resulting in a blue-shift in UV emission.

7.4 VIA (S)

The change in absorption threshold is crucial for efficient sunlight utilisation. Sulfur (S) doping in ZnO (S-ZnO) has received much attention because of its significant electronegativity and size discrepancy between S (1.8 nm) and O (1.4 nm) [247]. In S-ZnO, many oxygen vacancies (V_O) and zinc vacancies (V_Z) are produced. These vacancies will facilitate O_2 adsorption and the capturing of photo-induced electrons which sequentially produce high photocatalytic efficiency [248]. PL is a useful technique for studying S doping in the ZnO lattice. Commonly, the PL spectrum of ZnO represents two bands: (1) 370–400 nm owing to the free exciton's recombination via the exciton's collision and (2) 450–550 nm owing to the recombination of electron-hole inhabiting singly ionized V_O [249]. The UV emission peak intensity decreased, indicating low recombination of photo-induced charge carriers in S-ZnO [250]. Cho et al. mentioned undoped nanowires emit strong UV near the band edge (375 nm) and weak visible emission near 557 nm [251]. The visible emission was improved compared to the UV emission as the concentration of thiourea was increased, and the emission peak was blue-shifted to near 517 nm, as predicted for S-ZnO [252]. Near band-edge emission (NBE) peaks only occur at higher S content, while both NBE and strong visible emission peaks occur at lower S content [253]. According to Xie et al., exciton absorption peaks with substantial blue-shift relative to bulk ZnS are due to the doped S and size effect [254]. When compared to undoped ZnO, Jothi et al. found that the bandgap value decreased for S-ZnO, but when the amount of thiourea

content was increased, the bandgap value of S-ZnO increased. Therefore, when compared to higher sulphur content addition, less sulphur content incorporation in ZnO induces effective changes in bandgap values [255]. Furthermore, small amounts of sulphur doping in ZnO appear to cause a noticeable valence band offset (VB). This is partially owing to the host forming Zn–S bonds, which affects the VB edge and narrows the bandgap [256]. According to Jaquez et al., there is a direct relationship between dopant concentration and the resulting red or blue-shift in wavelength [257].

8 Applications of doped ZnO nanostructures

The doped ZnO nanomaterials have been widely explored for making visible light photocatalysts, which is more advantageous over classical UV active photocatalysts, i.e. undoped ZnO. To overcome the issues related to photo-corrosiveness of ZnO and poor visible light absorption, ZnO could be suitably doped with metals or non-metals. For instance, the nanocomposite of N doped ZnO and graphitic-C_3N_4 for application as visible light photocatalyst [258]. The catalyst exhibited photostability under solar simulator for five consecutive catalytic cycles. Despite having wider band gap of ZnO, the nanocomposite of N-doped ZnO with g-C_3N_4 have drastically reduce the band gap. In most of the studies, the UV-Vis optical spectroscopy is found to be a very useful tool for finding the effect of dopants in the modification of ZnO bandgap. By using Tauc plot, the optical band gap of pure and doped ZnO could be easily calculated. Especially, for the ZnO nanomaterials due to higher surface to volume ratio that can exhibit improved physical and chemical properties and effect of dopants on bandgap modification could be clearly witnessed using XRD, absorption spectroscopy and Tauc plot, which could have direct influence on the optical, catalytic and sensing behaviour of ZnO. As discussed previously in the band gap modification, the p-type and n-type semiconducting nature of ZnO can be tuned according to the application of interest.

There are wide range of dopants viz., transition metals, metalloids, non-metals, rare earth metals could be easily introduced into the ZnO without compromising wurtzite crystalline structure of ZnO to improve n-type conducting property [5, 15, 51]. Kumari et al. (2019) explored the effect of S, N and C doping on ZnO towards photocatalytic activity [13]. Transition metal doped ZnO nanostructures are explored as a multifunctional material, which could act as photocatalysts, semiconducting materials, and sensor materials for detecting small volatile organic molecules such as acetone, ethanol, amines, formaldehyde and noxious inorganic gases such as CO, NO, NO_2 and for fabricating photovoltaic devices. By optimising the sol-gel synthetic method and choosing appropriate stabilising agent (for example, CTAB, citric acid, oxalic acid, urea, diethylamine, diethanol amine etc.), wide range of doped ZnO materials with variable nanostructures such as flowers, stars, rods, wires, sheets could be achieved to enhance surface area, gas sensing, catalytic, luminescence and visible light absorbing capacity when compared with bulk materials [14]. The template assisted sol-gel technique is very useful technique, since by using this technique nanostructured materials could be tailor made surface area, tunable nanoparticle size and shape, dopant concentration and tunable band gap could be achieved. Because the gas sensing and detector application using metal oxide (MO) semi-conductor nanoparticles is required tunable shape and bandgap. In addition to that these nanomaterials could be explored for making as energy storage devices, battery applications, electrode materials due to excellent physiochemical properties [9, 12, 52].

Nanomedicine is another important emerging field of research. The use of multi-functional nanomaterials could be applied as drug delivery system, photodynamic therapy, magnetic, sensors and imaging applications. Among the bionanomaterials, ZnO is possessing an important place in the list of biocompatible nanomaterials. Because of its biocompatibility, doped ZnO nanomaterials have found many applications in the biomedical field. Due to higher surface area and surface functionalisation, the nanoparticles could be act as excellent drug carriers and capable delivering the drug to specific target. Since the doping process is tunable, ZnO with desirable photo and physiochemical properties such as magnetic, fluorescence, bandgap engineering, photocatalytic and morphological modification could be achieved. Consequently, doped ZnO nanomaterial could be used in MRI, fluorescence bioimaging, anti-tumor and anti-microbial applications [10]. Functionalised QDs of ZnO doped with transition metals and rare earth metals have found wide applications as biosensors, bioimaging materials, anti-microbial agents, photodynamic and cancer treatment in the medical field [15].

8.1 Optical devices

Thin films of Sn, In and Al doped ZnO nanoparticles prepared using plasma technique have found to possess highly transparent and conducting nature, could be cost effective replacement for ITO conducting thin films [259]. The nanocomposite prepared as multi-layer nanolaminates comprising Cu^{2+} loaded ZnO and Bi^{3+} loaded ZnO for the application as visible range high reflectivity optical mirror [260]. Cu^{2+} doped ZnO and Bi^{3+} doped ZnO prepared by sol-gel method and deposited as the individual layer over n-type Si(100) using spin coating technique. X-ray diffraction and AFM study indicated that both Cu^{2+} and Bi^{3+} doped ZnO layer showed wurtzite crystalline structure with uniformly distributed grain size around 27.6–35.2 nm. The multi-layer laminates showed decrease in optical bandgap of 2.44 eV as compared to pure

ZnO. According to the optical reflectance study, Cu doped ZnO showed more reflectance as compared to Bi doped ZnO and undoped ZnO due to decrease in crystallite size upon Cu doping. On the other hand, 6 layers of the Cu^{2+} doped ZnO and Bi doped ZnO multiple layer mirror showed a high reflectivity of 99% at wavelength range from 550 to 750 nm. In addition, three bilayers of Cu doped ZnO and Bi doped ZnO showed very high photoluminescence and high reflectance.

There are many attempts have been paid towards development of various types of metal ZnO for the application in the UV photo detector/sensor [51] and Perovskite/ZnO UV-vis sensor applications [261]. The photoconductive sensor performance of ZnO doped with Li^{+}, Mg^{2+}, Al^{3+}, V^{5+}, Cu^{2+} and Ag^{+} metals have been analysed. The photoconductive nature of metal doped ZnO have been evaluated in terms of metal ion doping concentration, photocurrent stability, photo-response and reproducibility. The metal doped ZnO having variable nanostructures synthesized using sol-gel method. Many of the investigations stated that increasing concentration of metal ion doping improving UV photosensitivity, photostability and reduced the response time. Probably this is because of the metal ion substitution in the place of Zn^{2+} sites, which led to additional free charge carriers and improved the photoconductivity and sensitivity. Thus, the metal ion doped ZnO showed the enhanced photocurrent generation for UV detection.

Photoluminescence behaviour of ZnO nanoflowers doped with various loadings of Fe^{2+} have been studied and luminescence intensity with respect to the dopant concentration also evaluated [262]. Diffraction pattern study confirmed wurtzite crystalline structure of Fe doped ZnO. Interestingly, the morphological study of Fe doped ZnO nanopowders showed flower like structure of nanopowders with average crystallite diameter and length around 250 nm and 5 mm respectively (Figure 4).

The photoluminescence (PL) study revealed that the luminescence intensity significantly decreased at 1.0 and 1.5% Fe doping whereas the PL intensity increased while increasing Fe doping to 2.0 and 2.5% without change in the emission wavelength.

The rare earth doped ZnO nanowire containing 3, 6 and 9 wt% of Nd^{3+} doped ZnO nanowires having 3-5 nm width using sol-gel method in 2-methoxyethanol as solvent and ethanolamine as stabilising agent have been prepared [57]. The diffraction study confirmed the nanowire formation from the occurrence of (002) diffraction peak with high intensity. The incorporation of Nd showed red shift in absorption maxima and gradually reduced the optical bandgap to 3.18 from 3.33 eV. The PL spectra of Nd:ZnO thinfilms showed incremental luminescence intensity and red shift with respect to increase in Nd loading (Figure 5).

The UV photosensing behaviour of Nd doped ZnO tested using I-V characteristics. Nd doped ZnO showed higher photocurrent and increased from 5.37×10^{-7} to 3.77×10^{-6} A with respect to increasing concentration of Nd dopant. The increasing photocurrent could be speculated due to generation of a greater number of charge carrier upon exposed UV light.

Ionic liquids mediated synthesis of Cu^{2+} doped ZnO achieved nanorods and flower like nanostructures, which is most preferred nanostructure for studying sensor and optical applications, where higher surface area is required [263]. Diffraction study revealed that wurtzite crystalline structure retained before and after incorporation of Cu dopant. However, the blue shift in UV-Vis absorption pattern is observed. The non-linear optical activity of Cu doped ZnO nanorods and flowers have been studied using Z-scan experimental setup. The study revealed that non-linear absorption (NLA) and non-linear refractive index (NLR) have been measured to be 5.5697×10^{-3} (cm /W) and 10.3254×10^{-8} (cm^2 /W) respectively using 55 mW laser and sample at 532 nm.

Besides UV-Vis photodetection and photoluminescence, thermoluminescence properties of 1-3% Mg^{2+} doped ZnO have been explored [264]. Mg-doped ZnO nanoparticles

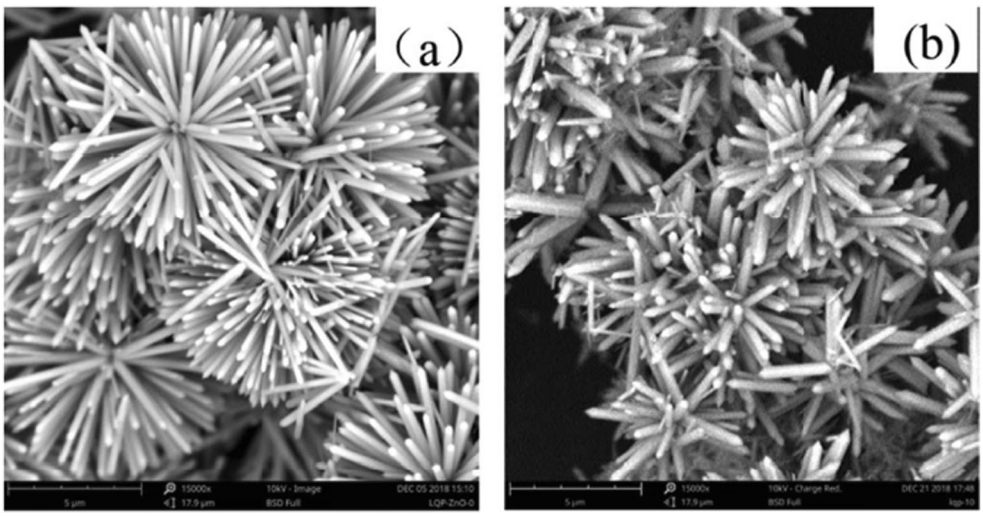

Fig. 4 SEM image of (**a**) pure ZnO and (**b**) 1.0% Fe doped ZnO (Adopted with permission from [262] with permission)

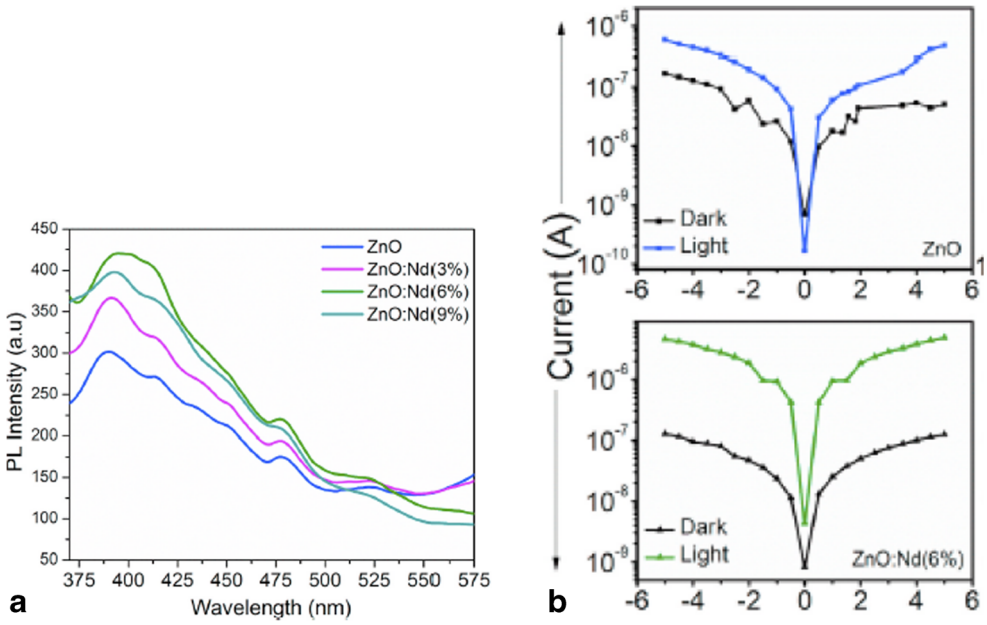

Fig. 5 (**a**) Photoluminescence spectra; (**b**) Semi-log I–V characteristics of the fabricated pure ZnO and 6% Nd doped ZnO photo sensor measured in dark and illumination conditions at a bias voltage between − 5 and 5 V prepared using different Nd doping concentrations (Adopted from [57] with permission)

prepared by sol-gel method using EDTA. X-ray diffraction studies revealed hexagonal wurtzite crystalline structure maintained for up to 3% Mg^{2+} doped ZnO. By using Scherrer equation, the crystallite size calculated and found to be while increasing dopant concentration from 1 to 3% resulted in decrease the crystallite size from 48.5 to 38.7 nm for 3% Mg-doped ZnO. When compared with pure ZnO, Mg^{2+} doped ZnO nanomaterials showed higher thermoluminescence curves at 280 to 330 °C. With respect to dopant concentration, 1% Mg-doped ZnO sample exhibited higher TL intensity with excellent reproducibility when compared with 2% and 3% Mg-doped ZnO samples.

8.2 Photovoltaic devices

The crisis for energy is a global issue because of the high demand and the solution is the low-cost, highly efficient energy harvesting device from the renewable energy sources. To meet the high demand of energy requirement there is plenty of research and development activities have been going on high-efficiency solar cells for decades, and few of the technologies have been made into commercial success. However, the novel materials with effective conversion of solar energy are needed to overcome the issues associated with the current technologies. Among the many semi-conducting metal oxides, ZnO nanoparticles are found to be applied as excellent electron transport layer in the fabrication of photovoltaic devices. It is used in the form of the compactor nanostructured layer deposited on the cathode to facilitate electron extraction from the device [265].

Organic–inorganic hybrid halide perovskite solar cells (PVSCs) have attracted great attention because of their economical fabrication cost, stability, achieving expected solar power conversion efficiency up to 22.1%. The high performance of PVSCs is associated with the excellent physico-chemical properties of perovskite materials, being an efficient solar light absorber. In addition, these materials having a direct bandgap, high absorption coefficient, and excellent electron carrier transport power conversion efficiency (PCE) of 22.1% [266]. One of the essential properties is the long-term photo and thermal stability towards exposure to sunlight, which is a frightful challenge for the researchers. The most commonly used solar cells consist of an electron transport layer (ETLs) and the perovskite layer is a hole transfer layer. The dual functionality of ETLs as, either hole blocking or an electron transport layer, which enhances and generates the photocurrent by suppressing the recombination rate of charge carriers [267]

ZnO nanoparticles have been a good replacement for expensive ITO plates because of transparency with higher mobility for electron and strong luminescence at ambient temperature. However, the efficiency of perovskite-based ZnO as ETLs is relatively low due to the chemical instability of ZnO in acidic medium this can be overcome by doping Sn which has a wide-bandgap [268]. The use of Sn^{4+} doped ZnO nanocomposite has shown a higher photocatalytic activity when compared with individual oxides of Sn and Zn, because of minimising the recombination rate of electron-hole. Kadem et al (2019) synthesized Al doped ZnO (AZO) transparent layer for organic solar cell application [269]. In which, the organic layer containing PCDTBT: PCBM blends coated on Al doped ZnO using sol-gel method as an electron transport layer. The benefits of doping by Al on the morphological and photovoltaic properties of Al doped ZnO layer were investigated. The doping of Al influenced growth of crystallites size, which resulted in different surface morphology and

characteristics. Al doping in ZnO broaden the band gap with improved charge carrier density. The use of 0.5% Al loaded AZO as an active layer showed photovoltaic performance up to 3.24% as compared to the reference device, which showed efficiency of 2.9%. Koksal et al. (2021) have attempted to enhance photovoltaic performance by using Al and Ga co-doped ZnO for heterojunction diode application [270]. The diode, which made of Al and Ga doped with ZnO (AGZO) showed an improvement in the diode device operation. It shows remarkable rectification properties with a $I_{forward}/I_{reverse}$ of 8146 at ± 4 V (Figure 6). Compared to the values diode performances for undoped, Al-doped and Ga-doped ZnO-based devices in the literature, undoubtedly, our results are promising, indicating that co-doped layers should also be considered in fabrication of thin-film-based diodes.

8.3 Photocatalysis

Due to the modification in natural bandgap of ZnO, doped ZnO semi-conductor acts as an active visible light photocatalyst for the organic pollutants degradation. Some of the metal doped ZnO photocatalysts have explored for reduction of CO_2 under solar light [271]. For instance, Ba-Abbad et al (2013) synthesised Fe doped ZnO for the application as visible light photocatalyst for the degradation of organic pollutant like 2-chlorophenol. The photocatalytic abilities of doped ZnO have been enhanced with respect to increasing Fe^{3+} dopant concentration [272]. The doped ZnO nanoparticles were prepared using an economical sol–gel synthetic method. The X-ray diffraction study revealed that ZnO exhibited in wurtzite, hexagonal crystalline structure in which the Fe^{3+} ions well incorporated into the ZnO crystal lattice. The ZnO crystallite size decreased from 18 to 12 nm as

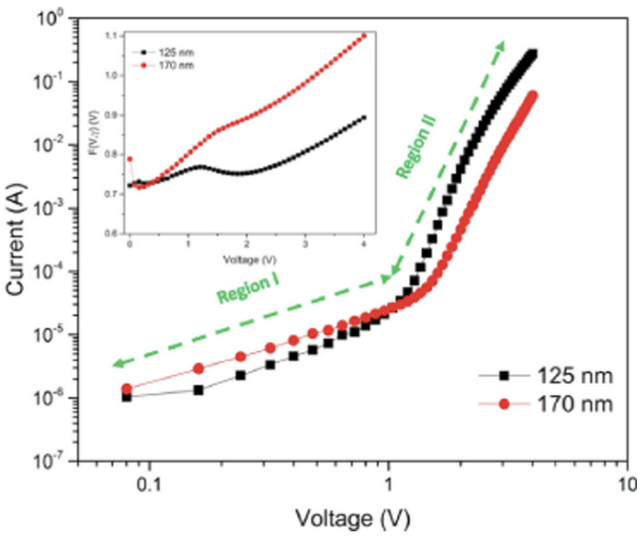

Fig. 6 I–V characteristics of Al and Ga co-doped ZnO diode (Adopted with permission from [270])

compared to pristine ZnO, when Fe^{3+} concentration increased from 0.25 to 1 wt.%. Further, the UV-Visible spectral studies showed that the dopant caused red shift in absorption maxima, which interpret the decline in the optical band gap to 2.65 eV for 1wt% Fe doped ZnO. The visible light photocatalytic efficacy has been examined based on the 2-chlorophenol degradation in a synthetic wastewater under solar radiation. The ZnO nanoparticles doped with 0.5 wt% of Fe^{3+} dopants showed improved photocatalytic activity with maximum performance. Smaller crystallite size and lower optical band gap are essential parameters to enhance activities of Fe–ZnO samples under various concentrations of Fe^{3+} ions when compared with undoped ZnO.

The waste generated from the synthesis and dyeing of synthetic dyes pose a critical impact on the environment and health and major cause for both water and soil pollution. The eco-friendly and economical solution for treating the contaminated wastewater is using the photocatalysts. For more than decade, nanoparticles have been studied for better degradation of dyes, especially TiO_2 and ZnO-based photoredox catalysts [266].

The semiconductor metal oxide nanoparticles when exposed to light can generate electron-hole pairs which undergo series of photo redox reactions to produce hydroxyl groups from decomposition of water as the main oxidizing agent to disintegrate the organic molecules of the dye or any other organic pollutants into smaller molecules like CO_2 and H_2O [273]. However, doped zinc oxide exhibits exceptional photostability and higher quantum efficiency in the UV-Vis region, the challenges posed by pure ZnO, and other metal oxides could be gradually overcome by gaining attention as a possible alternative material for photocatalytic degradation of organic polluted water under visible light or solar light [274, 275]. This is because doped ZnO nanomaterials displayed good photoluminescence and photoactivity behaviour due to relatively higher surface area and quantum yield when compared with other metal oxides [5]. In addition, it is observed that doped ZnO has a high tendency of showing higher photoreaction and decomposition rates leading to the generation of hydroxyl radicals which are the major oxidizing species. Especially Sn doped ZnO nanocomposite which has efficient charge separation properties. Improved photocatalytic activity has been observed in the case of Sn doped ZnO compared with the pure ZnO nanoparticles [276, 277].

Kong et al (2017) reported nitrogen doped ZnO for application as photocatalysts mediated under visible light for the decomposition of organic pollutants such as methylene blue and phenol [258]. The nanocomposite photocatalyst comprising N doped ZnO and graphitic-C_3N_4 have been prepared sol-gel method using urea as a nitrogen source. X-ray diffraction showed reduction in crystallite size from 45.8 to 38.6 nm due to doping with nitrogen without modification in the wurtzite crystalline structure of ZnO [258]. In addition, for

the N doped ZnO the optical bandgap is declined to 3.10 from 3.21 eV. Further, the nanocomposite of N incorporated ZnO with g-C_3N_4 showed broader absorption in the visible region and drastically reduced the optical bandgap to 2.73 eV. Whereas the nanocomposite of undoped ZnO with g-C_3N_4 showed the bandgap up to 2.85 eV. The degradation of phenol/methylene blue using nanocomposites studied under solar simulator. The degradation studies revealed that N-doped ZnO/g-C_3N_4 nanocomposite degraded methylene blue up to 90% within 60 min with higher degradation rate when compared with undoped ZnO nanocomposite. The enhancement in the degradation rate due to combined effect of N-doped ZnO/g-C_3N_4. In addition, the catalyst could be recycled up to reaction cycles without losing the catalytic efficiency. Hence, the nanocomposite of doped ZnO with g-C_3N_4 would be viable option for fabricating visible light photocatalyst.

The photocatalytic and anti-bacterial behaviour of Mg^{2+} doped ZnO nanoparticles, which obtained using co-precipitation process [278]. Doping of Mg^{2+} in ZnO not altered the hexagonal wurtzite crystalline nature of ZnO which displayed by X-ray diffraction studies. In addition, the incorporation of Mg^{2+} increased the crystallite size from 24 to 90 nm for 7.5 mol% doping with Mg^{2+}. The UV-Vis spectroscopic studies showed red shift in absorption maxima, which indicates that decrease in optical band gap from 3.36 to 3.04 eV when increasing Mg^{2+} doping concentration. Photocatalytic efficacy of Mg^{2+} doped ZnO studied using degradation of Rhodamine B. The study revealed that the maximum degradation is observed up to 78% for 7.5% Mg-doped ZnO NPs under UV-Vis irradiation.

The photocatalytic efficacy of Mn^{2+} loaded ZnO nanofibres synthesised using electrospinning technique (Figure 7). In this study, nanofibres of ZnO loaded with 5, 10, 15 and 50 at% of Mn^{2+} fabricated using electrospinning followed by annealed at 800 °C [279].

X-ray diffraction revealed wurtzite structure of Mn doped Zn nanofibre and showed incorporation of Mn from the diffraction pattern as observed 50 at% of Mn doping. The photocatalytic decomposition of Rhodamine B showed that the nanocomposite containing 50:50% of MnO–ZnO displayed higher photocatalytic performance because of increased quantum efficiency up to 7.57%, whereas pure ZnO showed only 0.16% under visible light.

ZnO is widely applied photocatalytic reactions because of higher photosensitivity in UV-Vis region and possess optimum band gap and doped ZnO nanomaterials displayed exceptional chemical and physical stability in the presence of light [276]. For example, photo-corrosiveness is a kind of setback for using pristine ZnO as photocatalysts for the organic pollutant degradation. The nanoparticles of ZnO doped with Sn^{4+} synthesised using precipitation process. Diffraction analysis revealed inclusion of Sn^{4+} ions into wurtzite framework of ZnO. Sn loaded ZnO showed excellent degradation of methylene blue when compared with pure ZnO and 95.41% of photocatalytic efficiency is observed.

Templated assisted sol-gel method used for synthesis of mesoporous Nd doped ZnO for the pharmaceutical pollutant degradation study [280]. Nd/ZnO mediated of photolytic decomposition of tetracycline (TC) promoted on exposure to visible light much higher when correlate with pure mesoporous ZnO nanoparticles (NPs) and commercially available photocatalyst P-25. The efficiency of photolysis using mesoporous 3%Nd_2O_3/ZnO reached up to 100% within 2 h, whereas pure mesoporous ZnO and P-25 showed only about 4 and 10% respectively in the degradation of TC. The mesoporous 3%Nd_2O_3 doped ZnO photocatalysts enhanced photocatalytic performance, photodegradation rate value maximum of 8.8 and 16.3 times that of compared to pure ZnO and P-25. This exceptional phenomenon could be due to better separation of photogenerated charge carriers, which resulted in heterojunction constructed between interface of Nd_2O_3 and

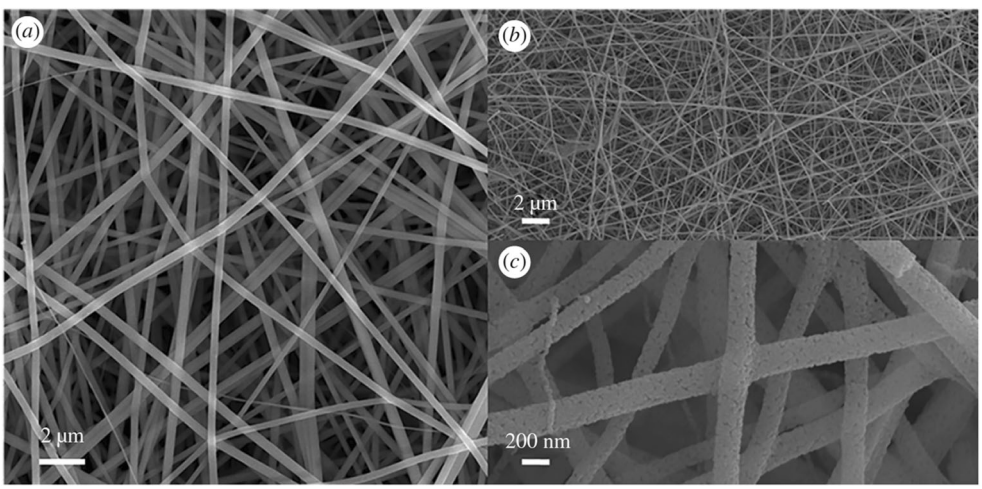

Fig. 7 SEM images of (**a**) as-spun nanofibres, (**b**) the MnO–ZnO nanofibres annealed at 800 °C for 1 h in NH_3 and (**c**) enlarged view of the fibres. (Courtesy from [279] and shared under Creative Commons Attribution 4.0 International Public License)

ZnO. Further, the 3%Nd_2O_3/ZnO catalysts showed adequate photo stability for five repeated degradation cycles.

Co doped ZnO prepared using coprecipitation method for studying UV irradiation promoted photolytic degradation of methylene blue as a model pollutant [281]. X-ray diffraction studies revealed that the substitution of Co ion in the place of Zn in wurtzite structure is observed. In addition, the effect of doping on crystallite size showed that the size of crystallite size shrinks from 42.90 to 17.38 nm for 10 mol% Co doped ZnO. Further, the lattice parameters revealed an increasing trend in doped ZnO which indicated the inclusion of Co ions into ZnO framework. The decrease in optical bandgap is observed after Co doping. The pure ZnO showed band gap 3.22 eV, whereas it is gradually reduced to 3.07, 2.87, 2.61 and 2.59 eV for 4, 6, 8 and 10 mol% Co/ZnO. Interestingly, when correlate with higher Co/ZnO, 4 mol% Co doped ZnO showed higher photocatalytic degradation efficiency up to 100% and reached maximum methylene blue degradation as compared to the pure ZnO with in 60 min [281]. Further, the study stated that increasing doping concentrations of Co showed a decrease in photocatalytic efficiency.

La doped ZnO nanoparticles containing 1, 5 and 10 mol% of La prepared by co-precipitation for the dyes such as methyl orange and rhodamine photolytic degradation promoted by UV irradiation [58]. According to diffraction studies, the incorporation of La not affected the wurtzite framework of ZnO. The crystallite size reduced to 20.12 nm while increasing concentration of La doping from 1 to 3 mol%. According to UV-Vis studies, very marginal change in the optical bandgap for La doped ZnO is observed and the optical band gap was found to be 3.30, 3.28 and 3.30 eV for 1, 3 and 5 mol% La doped ZnO respectively. The photodegradation of methyl orange, Rhodamine B and picric acid showed 1 mol% La doped ZnO found to be efficient catalyst. The catalyst showed degradation efficiency up to 100% for methyl orange and Rhodamine B and 90% for picric acid and reached maximum degradation rate within 120 min contact time.

The degradation of methylene blue as a model pollutant using Ce doped ZnO under UV radiation in a batch type reactor [282]. By adopting the sol–gel combustion method, Ce doped @ 1, 3 and 5 mol% in zinc oxide (CZO) nanoparticles have been synthesized. XRD studies revealed that hexagonal wurtzite structure exhibited by the CZO nanomaterials. As compared to pristine ZnO, the crystallite size of 1 mol% Ce doped ZnO increased from 57 to 84 nm as calculated using Scherrer equation. In addition, due to larger ionic size Ce as compared to Zn showed the lattice expansion as observed from diffraction studies. The optical bandgap slightly decreased to 3.20 eV after Ce doping when compared with pure ZnO. The photocatalytic efficacy evaluated using methylene blue revealed that 5 mol% Ce doped ZnO showed higher degradation efficiency up to 65.8% during 300 min contact time as compared to pure ZnO, and 1 and 3 mol% Ce doped ZnO.

Mirzaeifard et al. (2020) reported the visible light the photocatalytic efficacy on 0.5–17.4 wt% sulphur doped ZnO using Rhodamine B as a typical pollutant [273]. The sulphur containing ZnO prepared using sol-gel hydrothermal technique and using thiourea as sulphur source. The diffraction study performed to prove that the Wurtzite structure is maintained up to 7.8 wt% of sulphur, whereas the crystalline nature is collapsed at higher loading of sulphur. In addition, at higher loading the formation of ZnS is observed from the diffraction studies. The crystallite of S doped ZnO is reduced from 35 to 15 nm for sulphur content increased from 0.5 to 11.9 wt%. The UV-Vis absorption study showed red shift in absorption maxima and subsequently the band gap is reduced to 3.02 from 3.33 eV with respect to increasing concentration of sulphur. Among the S-containing samples, 0.5 wt% S doped ZnO degraded RhB with 100% @ 5 ppm and pH @ 5 within 90 min of contact time. In addition, 0.5 wt % S-doped ZnO showed degradation up to 53% of the phenol in 3 h at the same pH. The recycling study of the S (0.5 wt%)/ ZnO can be reusable up to five cycles under optimized conditions and after five successive degradation cycles efficiency was decreased to 92% [273].

Sr doped ZnO showed a redshift as well as decrease in PL intensities when compared with pristine ZnO as well as the crystallite size increased from 20 to 60 nm, when increasing dopant concentration from 1 to 7 Mol% of Sr. The redshift indicates the decline in the optical bandgap from 3.34 to 3.17 eV. According to the report, the decrease in PL intensity and redshift stated that effective prevention of electron-hole from recombination. The recombination of electron-hole is minimised and the photocatalytic behaviour of the semi-conductor is enhanced [283]. Under visible light, methylene blue photocatalytic degradation catalysed using Sr loaded ZnO revealed that 3 at% of Sr loaded ZnO recorded higher photocatalytic efficiency up to 97% within 30 min contact time.

8.4 Sensor applications

The detection of volatile organic compounds and noxious gases at low level using sensors made from nanomaterials would improve the quality of human life and provide higher healthy and safely living environment [9, 284, 285]. As we understand, the major cause of pollution is harmful gases from the combustion of fossil fuels and toxic chemical substances to the atmosphere. The release of harmful gaseous substances not only pollute the surroundings but also cause severe threat to the hygiene and health of all the living beings. In this scenario, the development of more sensitive and rapid volatile compounds/gas sensors for the detection with higher selectivity received enormous interest vested in the nanomaterials [4].

Breath sensors based on metal oxides having enormous potential in early stage and rapid detection of many volatile disease biomarkers such as NO, H_2S, isoprene, acetone and formaldehyde [286]. Among various gas sensors, the zinc oxide semiconductor gas sensors having transition metal doped zinc oxide nanoparticles as sensing layer consumes less expensive and operates at room temperature with a great level of sensitivity and selectivity [25, 287, 288]. For instance, Ag doped ZnO as humidity sensor [289], electrospun SnO_2 doped ZnO nanofibres for the detection of H_2S [290], PbS QDs doped ZnO nanorods for ethanol sensing [291] , Ag doped ZnO nanoflower for NO sensing [292], Au loaded ZnO nanoparticles for Toluene gas sensor [293], Fe doped ZnO/ graphene oxide nanocomposite for formaldehyde sensing [294], nanocomposite of ZnO-MoS_2 for low temperature acetylene sensor [295], Pd doped nanoparticles for NH_3 gas sensing [296], Pd doped ZnO electrospinning nanofibres for CO sensing [297] . Most of the studies explored that doped ZnO having interesting nanostructures useful for the detection of toxic and flammable volatile organic substance and inorganic gases such as CO, NO, NH_3 and H_2S.

The application of chemically resistive gas sensors for the volatile organic pollutants and other noxious substance is inevitable due to emerging of strict monitoring of indoor air quality in many industrial sectors as well as indicator for environmental air pollution [14, 298–301]. In addition, due to the higher surface area to volume ratio and surface functionalisation, the nanosensors could be efficient detectors, which has tremendous opportunities in the medical field. As we are well aware that ZnO is an interesting n-type low-cost multifunctional metal oxide with bandgap of approximately 3.37 eV, and there are many investigations reported the application of ZnO and doped ZnO, and their nanocomposites as an economical efficient gas or volatile compounds sensing material because of excellent electrical performance, fast response to lower detection limit with shorter recovery time and enduring stability when compared with other semiconducting metal oxides under thermal [25, 295, 302] and light driven gas sensing applications [303]. Nevertheless, to continuously improve the sensor performance, modified ZnO with noble metal like Pd nanoparticles has been reported and demonstrated higher response and sensitivity in the light assisted NO_2 sensing [304].

The possible applications of various metal doped ZnO with different nanostructures as the gas sensor have been investigated. As discussed in many studies, the doped ZnO is a typical MOS, which proven to be a potential material for applications in the detection of toxic gas. On the other hand, the metal doping is one of efficient method for increasing the sensor performance of ZnO materials with higher selectivity and sensitivity. Umar et al (2018) synthesized Ag doped nanoparticles for sensing of ethanol [305]. The crystallite size of Ag doped ZnO observed at average of 20 ± 5 nm and wurtzite crystalline structure retained after Ag doping. The Ag doped ZnO showed ethanol detection limit 200 ppm. In another study, for ethanol and H_2S gas sensing capacity of Ag-doped ZnO nanoparticles fabricated at 1, 3 and 5 mol% Ag doping. Three mol% Ag doped ZnO showed fast performance with respect to response/ recovery for ethanol at 5 and 9 s, whereas maximum response time found to 298 at 10 ppm for H_2S gas [25].

Yoo et al. (2019) reported on Al doped ZnO for acetone sensing for industrial and breath analysis applications [28]. The study revealed that Al doped ZnO could serve as chemo resistive acetone vapour sensors. 1at% Al containing ZnO nanoparticles prepared using Flame Spray Pyrolysis method, which showed higher acetone sensing performance when compared with pure ZnO at limit of detection 10 ppm acetone. Furthermore, the 1at% Al doped ZnO nanoparticles showed more than 90% of sensing response when acetone concentration reduced from 10 to 1 ppm with higher selectivity for acetone as compared to other compounds such as NH_3, isoprene and CO. The doping of Al in ZnO NPs is expected to create more oxygen vacancies than pure ZnO using FSP method. Because of the oxygen vacancies, more oxygen ions could be adsorbed on the surfaces of NPs and may react with acetone molecules.

The thin films of ZnO containing 0.5, 1.0 and 1.5 at% of Sn^{4+} have been fabricated for the sensing of formaldehyde [29, 30]. The concentration of Sn dopant varied from 0.5, 1.0 and 1.5at%. The high prevalence of peak at 002 identified from diffraction study showed the formation of thin films. By using Scherrer equation, the crystallite size calculated to be 10.09, 33.36, 8.736 and 9.31 nm for ZnO thin film containing undoped, 0.5, 1.0 and 1.5 at% respectively for Sn^{4+} dopants. With respect to increasing dopant concentration, the decline in surface roughness is observed. The thin film fabricated out of 1.0at% Sn^{4+} loaded ZnO revealed detection at 3.4 ppb with 92% sensing performance for formaldehyde is found to be the maximum performance and in contrast only 50% sensing to formaldehyde displayed by undoped thin film. In addition, 1.0 at% Sn^{4+} doped ZnO thin film responded well within 4–10 s and recovered within 15–34 s, whereas pristine ZnO showed longer response and recovery time, valuably at 10–8 s and 38–207 s, respectively. For nine consecutive days, the thin film containing 1.0at% Sn incorporated ZnO showed sensing performance above 90% without losing the efficiency.

Wang et al (2020) explored three-dimensional ordered Au and In doped macroporous ZnO (3DOM ZnO:In) for ethanol sensing [26]. In this investigation, 3DOM Au–ZnO:In have been obtained using a polymeric colloidal template assisted by PMMA. The wurtzite crystalline nature of ZnO is shown by X-ray diffraction and crystallite size decreased from 12.74 to 11.56 nm, while increasing Au concentration from 0.025 to 0.075%. Due to larger ionic radius of Au (137 pm), the Au ions not able to be doped in ZnO lattice, unlike In ionic radius (80 pm) comparable with Zn ionic radius (74 pm), which

doped in ZnO lattice. However, the study states that Au ion uniformly distributed in the highly ordered three-dimensional porous morphology. The tendency for sensing ethanol capacity have been probed and proved that 0.050 mol% Au-loaded 3DOM ZnO/In found to possess greatest sensitivity up to 100 ppm at 250 °C with excellent selectivity and stability.

8.5 Magnetic properties

By using sol-gel method, ZnO nanoparticles (NPs) and nanorods (NRs) containing Co as dopants were synthesized. SEM morphology of the Co doped ZnO revealed that presence of 5% dopant resulted mostly as nanoparticles, whereas 10% Co doped ZnO is exhibited nanorods morphology [306]. UV-Vis study showed increase in optical density upon doping with Co and blue shift in absorption maxima is observed and optical band gap is increased 3.24 from 3.10 eV upon 10% Co doping in ZnO. The optical band gap widening is speculated with the particle size contraction upon doping. The magnetic behaviour has been studied using field-dependent magnetization measurements at 300 and 2 K. The study revealed that ZnO NPs is diamagnetic nature, whereas 5 and 10% Co doped ZnO NPs exhibited paramagnetic behaviour at 300 K and at 2 K, Co-doped ZnO NPs showed superparamagnetic behaviour. In addition, the ferromagnetic character is observed at lower field region.

Aggarwal et al. (2018) prepared Gd-doped ZnO nanorods with objective of studying ferromagnetic behaviour before and after doping [307]. Gd incorporated ZnO nanorods have been prepared using sol-gel hydrothermal method using CTAB as stabilizing agent. X-ray diffraction study proved that the inclusion of Gd led to replacement of Zn in ZnO lattices, which reduced the crystallite diameter from 28.41 to 20.03 nm because of the larger ionic radius of Gd when compared with Zn. UV-Vis study showed that incorporation of Gd reduced the bandgap of ZnO from 3.32 to 3.27 eV according to UV-Vis studies. M-H plot of ZnO and Gd-ZnO showed pure ZnO nanorod exhibit weak ferromagnetism and Gd doped ZnO nanorod exhibit long range ferromagnetism at room temperature.

Thamaraiselvan et al (2018) studied ferromagnetic behaviour of Mn doped ZnO thinfilms [308]. On glass substrates, the thin films of Mn doped ZnO were grown using hydrothermal process and hexamethylene tetramine as a stabilizing agent. The ferromagnetic behaviour of Mn doped ZnO thinfilm has been studied with the help of vibrating sample magnetometer (VSM). The study showed that ferromagnetic behaviour of ZnO thin film reduced upon concentration of Mn dopant increases. The ferromagnetic behaviour of V doped ZnO has been investigated [309]. This investigation attempted to explore ferroelectric behaviour of ZnO because of its non-centrosymmetric nature of wurtzite structure of ZnO. The study speculated that the ferroelectric behaviour could be altered by doping with transition metals having larger ionic radius than Zn. Thus, vanadium is selected as dopant to study the ferroelectric nature of ZnO. Diffraction X-ray investigation displayed that strain have been induced in wurtzite structure of ZnO with 5% doping with Vanadium due to difference in ionic radius between V and Zn. Further, the magnetization behaviour of V doped ZnO thin films studied at room temperature revealed that ZnO is developed ferromagnetic nature after doping with vanadium. The magnetic moment observed is 0.8 mB per vanadium in doped ZnO.

The Cu doped ZnO nanoparticles and studied its ferromagnetic nature using VSM technique [310]. ZnO nanoparticle doped with 0.05 mol% of Cu have been prepared by sol-gel auto-combustion approach in the sight of citric acid as a fuel. X-ray diffraction studies confirmed that Cu doped ZnO exhibit wurtzite crystalline structure. Further, the shift in diffraction peaks is observed due to substitution of Cu in ZnO lattice and crystallite size is reduced from 21 to 19 nm. The ferromagnetic behaviour of pure and Cu doped ZnO has been studied using VSM technique at room temperature. The study revealed that ZnO is paramagnetic, which arise due to Zn vacancies. On other hand, the Cu doped ZnO exhibited ferromagnetism due to extrinsic effect raised by incorporation of Cu and intrinsic effect raised by Zn and O vacancies in the Cu doped ZnO crystal lattices.

ZnO doped with 4, 6, 8 and 10% of Co have been synthesised using co-precipitation method, which involved two steps [281]. The diffraction X-ray studies revealed that the crystallite size reduced from 42.90 to 17.38 nm upon increasing Co doping from 0 to 10%. Further, the doping of Co decreased the optical band gap to 2.6 from 3.2 eV for 10% Co containing ZnO. Magnetisation properties studied at 300 K showed that pure ZnO possess weak ferromagnetic character because of the defects present in the lattices, whereas the study clearly demonstrated that Co doped ZnO possess ferromagnetic behaviour (Figure 8). Further, the study states that ferromagnetic nature increases with increase in Co doping.

8.6 Quantum dots

Singh et al. (2021) has made critical assessment on the metals belong to rare-earth and transition group doped quantum dots (QDs) of ZnO for application in optoelectronic, anti-bacterial and magnetic properties [15]. Undoubtedly, the doping of ZnO with transition metals would enhance optoelectronic and anti-microbial properties of ZnO due to modification of bandgap of ZnO. Rare earth metals of *4f* period such as Tb, Yb, Er, Eu, Ho and La doped ZnO QDs have been prepared by Sowik et al (2018) using sol gel method and studied photocatalytic and photoluminescence properties [56]. The doping of Eu, Er and La with ZnO resulted in increasing photocatalytic degradation rate of phenol up to 10% within 60 min. On the other hand, 0.18–0.45 mmol of La and Er containing ZnO

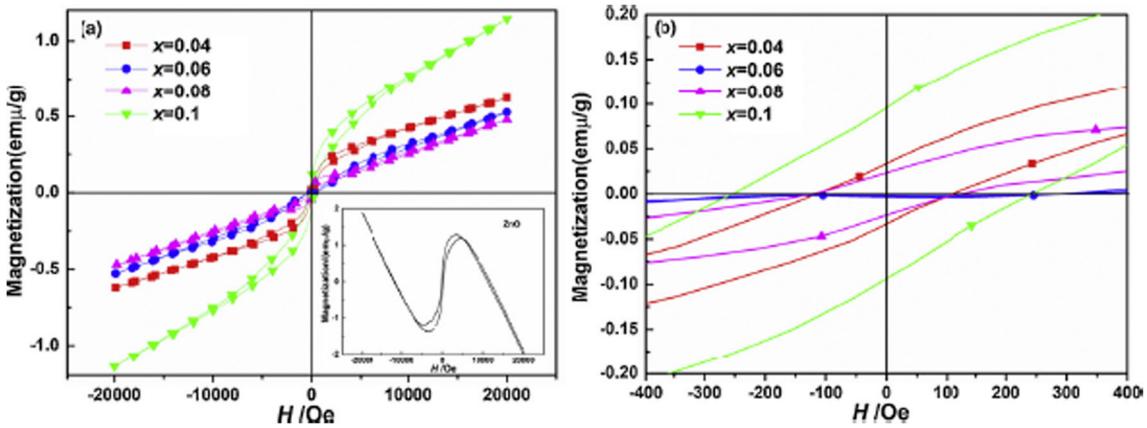

Fig. 8 (**a**) M-H plot for Co doped ZnO; (**b**) Magnified M-H plot (Adopted with permission from [281])

QDs showed higher photoluminescence intensity and 81% of quantum yield obtained for 0.45 mmol La doped ZnO QDs. Further, the study stated that photocatalytic behaviour is higher for ZnO QDs and for those showed lower PL intensity. In contrast, Pr doped ZnO QDs showed increasing photoluminescence intensity with increasing Pr dopant concentration [311]. Gd doped ZnO QDs have been synthesized for the application as diode material for laser. The doping of Gd in ZnO drastically narrowed the optical band gap to 2.80 eV. Further, the concentration of Gd showed positive influence on the luminescence intensity of ZnO QDs. In addition, the quantum yield increased from 31 to 94% upon Gd doping in ZnO QDs. Transition metal such as Cd doped ZnO QDs showed anti-bacterial properties due to formation of reactive oxygen species (ROS) during the degradation pathway on bacterial culture. The transition and rare earth metals doped ZnO QDs have found wide applications in the heavy metal ions detection, sensors for noxious gases, biosensor, bioimaging materials optoelectronic materials, photocatalysts, energy storage devices as well as nanomedicines such as anti-microbial agents and anti-cancer agents [15].

8.7 Electrochemical applications

Photoelectrochemical behaviour of ZnO makes it as an economically viable catalytic system for water splitting reactions and fuel cell applications due to its electron mobility and longer lifetime and lesser electron-hole recombination. 1D nanostructures with higher surface area ZnO nanowire showed excellent water splitting reactions driven by light. The photo-corrosive nature of ZnO can be reduced by doping or fabricating core shell nanoheterostructures, for instance, ZnO nanowire covered with TiO_2 nanotubes [312]. Core-shell structures of ZnO nanowires were coated with TiO_2 nanotubes prepared by sol-gel method (Figure 9).

Photoelectrochemical characterisation of ZnO@TiO_2 showed increased photocurrent density up to 0.20 mA cm^{-2} and solar to hydrogen conversion efficiency up to 0.07% as compared to TiO_2 nanotubes and ZnO nanowires. The combined effects of band edge positions of both the metal oxides and stable valence-conduction bands enhanced the reaction. The deposition of TiO2 crystals on ZnO surface reduced electron-hole recombination. 2D structure built from monolayers of $ZnCdO_2$ containing ZnO and CdO promoted visible light mediated water splitting reactions due to broad absorption in the visible light region and lowering of electron-hole recombination [313]. The valence band position of $ZnCdO_2$ and decreased electron-hole recombination is suitable for enhancing solar to hydrogen conversion efficiency as compared to ZnO and CdO monolayers. Shawuti et al (2020) prepared Li^+ and Co^{2+} codoped ZnO nanomaterial as an electrolytic material for fuel cell applications [314]. The nanoparticles doped with 10mol% of Co containing $Zn_{1-x}Co_xO$ have been doped with 5, 10 and 20 mol% of Li^+ using sol-gel technique. The ionic conductivity of doped ZnO could be tailor made by choosing appropriate amount of Li ion dopant. Reitveld refinements showed Zn ion substituted with Li ion, which improve the natural ionic mobility of ZnO semiconductor. The ionic conductivity and relaxation time studies showed the replacement of Zn ion with Li ion enhanced ionic mobility up to 0.0052 ± 0.0001 S cm^{-1} for 20 mol% Li loaded ZnO. The heterostructures fabricated from nanospheres of Mo and W co-doped $BiVO_4$/ZnO showed higher photoelectrochemical (PEC) response due to generation more excited charge carrier [315].

8.8 Biological activity of ZnO nanoparticles

Any material having biological compatibility, which could imply for biological applications. Photo-oxidizing and photocatalytic properties of doped ZnO which has impact on biological species. The anti-microbial agents derived from doped ZnO materials have been widely reported in many investigations against various pathogens in both micro and nanoscale. The interaction of nanosized ZnO with bacterial cell wall could be effectively achieved due to reduced particle size,

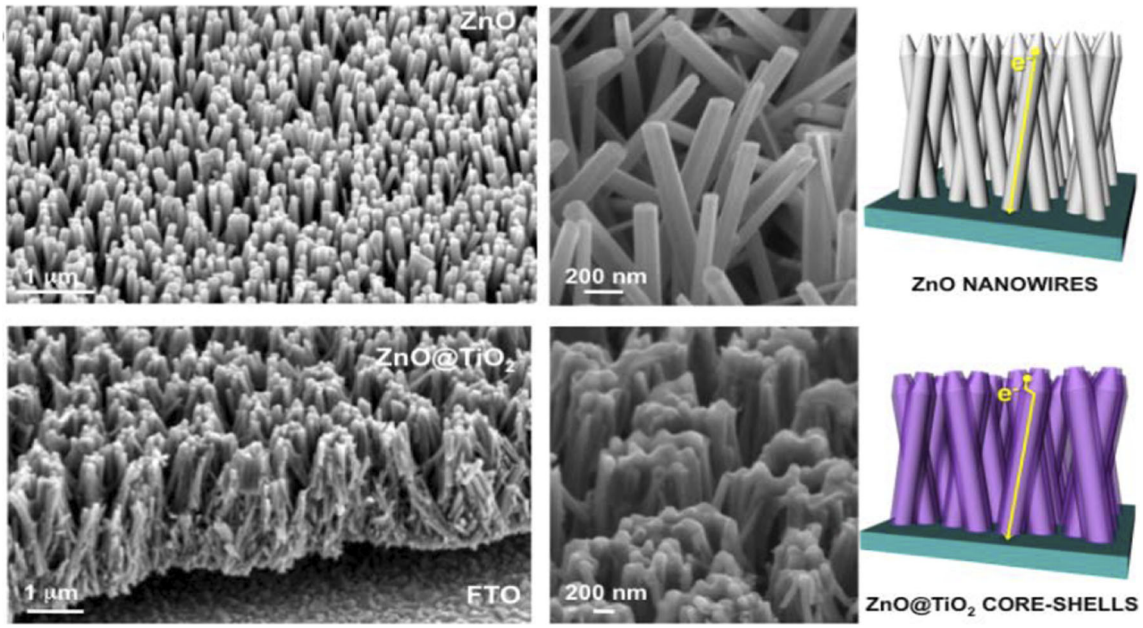

Fig. 9 45° tilted FESEM view of core-shell TiO_2 coated ZnO nanowires (Courtesy Ref. 312. This article is licensed under a Creative Commons Attribution-Noncommercial 3.0)

which is responsible for significant antimicrobial activities and enable nanosized ZnO entry into the bacterial core and subsequently disintegrate bactericidal mechanisms. The association of metallic nanomaterials and bacteria is mostly cytotoxic against bacterial cells, which could be used for designing antimicrobial agents for the food and pharmaceutical industries. On the other hand, ZnO nanoparticles are lesser toxic to human cells, which makes them be used as safer antibacterial agents, which is harmful to microorganisms and compatible to human cells.

Carofiglio et al (2020) explored applications of doped ZnO nanoparticles with respect to various aspects as nanomedicine [10]. The biological applications of doped ZnO nanomaterials are mainly affected by the nature of dopants and physicochemical properties including morphologies. The bandgap modification of pristine ZnO and photocatalytic behaviour has influence on doped ZnO for application in bio-imaging and anti-microbial properties. On the other hand, the morphological changes would support the nanoparticles biostability and degradation (please refer different morphologies of ZnO nanostructured materials achieved by various synthetic technique) [10]. Doped ZnO nanoparticles are known could be nanotheranostic materials since those are multi-functional biological system, where it could act as diagnostic as well as therapeutic applications. Anti-microbial activities of ZnO nanoparticles against pathogenic microbes could be effectively tuned by the type and stoichiometry of the dopants. Anti-microbial properties arise mainly due to alteration of photocatalytic and redox behaviour of ZnO by selecting appropriate dopants. In the aqueous medium, the formation of reactive oxygen species (ROS) by ZnO was due to photocatalytic activity, which can cause damage of bacterial cell wall and led to destruction of bacteria [7]. Anti-microbial activity against pathogenic bacteria using ZnO nanoparticles has received significant interest due to intervention of nanotechnology in biological efficacy of nanoparticles. The nanostructures of doped ZnO, due to higher specific surface area and smaller particle size, have displayed interesting anti-microbial properties with enhanced nanoparticle interaction with bacterial cell walls [316]. The dopants such as Ag^{+}, Cu^{2+}, Mg^{2+}, Al^{3+}, Fe^{3+}, Ce^{3+} containing ZnO nanoparticles have showed growth inhibition against such as *E. Coli, Salmonella, Listeria monocytogenes* and *Staphylococcus aureus,* which includes both gram-positive and negative variety[10].

Infectious diseases caused by pathogenic bacteria pose serious health threats, which received global attention to find all the possible ways to prevent from the infection. Because of prolonged use of classical anti-bacterial medicines, bacteria could generate antibiotic resistance. Thus, outbreaks and infections from pathogenic strains difficult to cure, the emergence of new bacterial mutations, and lack of suitable vaccine are global health hazards to humans. For instance, *Shigella flexneri* cause 1.5 million deaths annually, because of consumption of contaminated drinks and food by these bacteria [317]. For instance, Pathak et al. (2020) explored anti-bacterial and anti-fungal activity of Ce^{3+} doped ZnO against has been measured against *Staphylococcus aureus* and *Escherichia coli* and yeasts such as *Eremothecium ashbyii* and *Nadsonia fulvescens* [280] (Figure 10).

Pradeev Raj et al (2018) reported anti-bacterial activity of Mg^{2+} doped ZnO nanoparticles against both Gram-positive

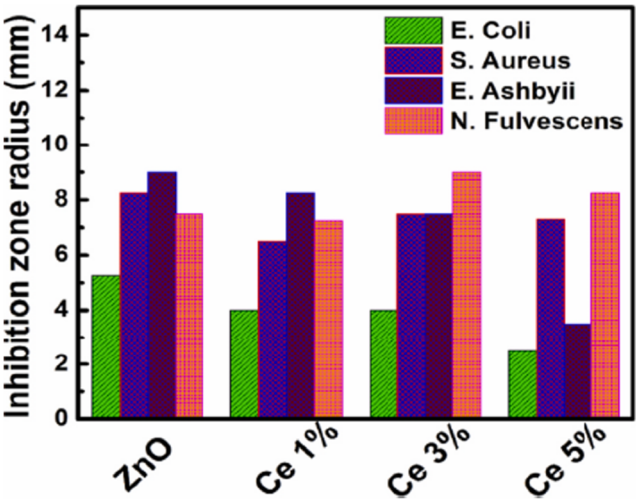

Fig. 10 Anti-bacterial and anti-fungal activity of Ce doped ZnO (Adopted with permission from [280])

bacteria (*S. aures*) and Gram-negative bacteria (*E. coli* and *Proteus*). The anti-bacterial study showed Mg/ZnO nanoparticles effective towards inhibition of both the type of bacterial growth. In addition, the level of inhibition of bacterial growth enhanced linearly with respect to Mg^{2+} dopant concentration, accordingly the decreased bandgap from 3.36 to 3.04 eV is observed. For instance, pristine ZnO nanoparticle showed zone of inhibition 9 ± 0.6 mm, whereas 2.5, 5 and 7.5% Mg^{2+} doped ZnO showed 13 ± 0.4, 16 ± 0.3 and 19 ± 0.3 mm respectively against *S. aures*. Apart from Mg doped ZnO, Sr doped ZnO nanoparticles containing 1, 3, 5 and 7 mol % of Sr have been explored for anti-bacterial activity against *E. coli* [281].

9 Future perspectives and conclusions

ZnO is a fascinating material with possibility of using it as a versatile metal oxide in various applications. From the perspectives of broadly available synthetic routes, ZnO could be grown in variable nanostructures including nanoflowers, hollow cages, nanowires and nanorods. p-Type and n-type conducting ZnO nanomaterials behaviour could be controlled respectively by using metal and non-metal (C, N and S) as dopants and the doping process with known stoichiometry could be synthesised by simple sol-gel hydrothermal and coprecipitation methods. The bandgap and nanostructures are crucial factors for enhancing the electronic and physicochemical characteristics of ZnO and both of them could be controlled by electronic nature of dopants and their composition and crystallite size.

The nanocomposites of doped ZnO with CNTs, g-C_3N_4, PANI and other MOs enhanced electronic behaviour such as band gap. The doped ZnO nanomaterials have found wide applications in photovoltaic, magnetic, photocatalytic, sensing and theragnostic materials. The luminescent doped ZnOs could be used in cosmetics, anti-microbial and cancer treatment. The doped ZnO nanomaterials with higher refractive index could significantly contribute for the fabrication of economical photosensors or optical devices. The visible light photocatalysis could be achievable using doped ZnO because of band gap modification. By utilising the wide spectrum of available dopants, doped ZnO nanomaterials with interesting nanostructures could be synthesised to meet the demand for many usefulness.

Declarations

Conflict of interest The authors declare no competing interests.

References

1. M.P. Nikolova, M.S. Chavali, Metal oxide nanoparticles as biomedical materials. Biomimetics **5**(2), 27 (2020)
2. N. Pal, Nanoporous metal oxide composite materials: a journey from the past, present to future. Adv Colloid Interf Sci **280**, 102156 (2020)
3. I. Şerban, A. Enesca, Metal oxides-based semiconductors for biosensors applications. Front Chem **19**(8), 354 (2020)
4. E. Fazio, S. Spadaro, C. Corsaro, G. Neri, S.G. Leonardi, F. Neri, N. Lavanya, C. Sekar, N. Donato, G. Neri, Metal-oxide based nanomaterials: synthesis, characterization and their applications in electrical and electrochemical sensors. Sensors **21**(7), 2494 (2021)
5. T.C. Bharat, S. Shubham, H.S. Mondal, P.K. Gupta, A. Singh, K. Das, Synthesis of doped zinc oxide nanoparticles: a review. Mater Today Proc **11**(2), 767–775 (2019)
6. H. Beitollahi, S. Tajik, F.G. Nejad, M. Safaei, Recent advances in ZnO nanostructure-based electrochemical sensors and biosensors. J Mater Chem B **8**(27), 5826–5844 (2020)
7. Y. Li, C. Liao, S.C. Tjong, Recent advances in zinc oxide nanostructures with antimicrobial activities. Int J Mol Sci **21**(22), 8836 (2020)
8. C. Yi, Z. Yu, Q. Ren, X. Liu, Y. Wang, X. Sun, S. Yin, J. Pan, X. Huang, Nanoscale ZnO-based photosensitizers for photodynamic therapy. Photodiagn Photodyn Ther **30**, 101694 (2020)
9. M.A. Borysiewicz, ZnO as a functional material, a review. Crystals **9**(10), 505 (2019)
10. M. Carofiglio, S. Barui, V. Cauda, M. Laurenti, Doped zinc oxide nanoparticles: synthesis, characterization and potential use in nanomedicine. Appl Sci **10**(15), 5194 (2020)
11. Z. Fallah, E.N. Zare, M. Ghomi, F. Ahmadijokani, M. Amini, M. Tajbakhsh, M. Arjmand, G. Sharma, H. Ali, A. Ahmad, P. Makvandi, E. Lichtfouse, M. Sillanpää, R.S. Varma, Toxicity and remediation of pharmaceuticals and pesticides using metal oxides and carbon nanomaterials. Chemosphere. **275**, 130055 (2021)
12. J.G. Reynolds, C.L. Reynolds, Progress in ZnO acceptor doping: what is the best strategy? Adv Condens Matter Phys **2014**, 1–15 (**2014**)
13. V. Kumari, A. Mittal, J. Jindal, S. Yadav, N. Kumar, S-, N- and C-doped ZnO as semiconductor photocatalysts: a review. Front Mater Sci **13**, 1–22 (2019)

14. P. Singh, R. Kumar, R.K. Singh, Progress on transition metal-doped ZnO nanoparticles and its application. Ind Eng Chem Res **58**, 17130–17163 (2019)
15. P. Singh, R.K. Singh, R. Kumar, Journey of ZnO quantum dots from undoped to rare-earth and transition metal-doped and their applications. RSC Adv **11**, 2512–2545 (2021)
16. S.P. Singh, Multifunctional magnetic quantum dots for cancer theranostics. J Biomed Nanotechnol **7**(1), 95–97 (2011)
17. W. Zhang, J. Hu, Y. Zhou, Y. Chen, F. Yu, C. Hong, L. Chen, H. Xin, K. Hong, X. Wang, Latex and a ZnO-based multi-functional material for cardiac implant-related inflammation. Biomater Sci **7**(**10**), 4186–4194 (2019)
18. M.K. Tabatabaei, H.G. Fard, J. Koohsorkhi, J. Mohammadnejad Arough, High-performance immunosensor for urine albumin using hybrid architectures of ZnO nanowire/carbon nanotube. IET Nanobiotechnol **14**(2), 126–132 (2020)
19. S. Karagoz, N.B. Kiremitler, G. Sarp, S. Pekdemir, S. Salem, A.G. Goksu, M.S. Onses, I. Sozdutmaz, E. Sahmetlioglu, E.S. Ozkara, A. Ceylan, E. Yilmaz, Antibacterial, antiviral, and self-cleaning mats with sensing capabilities based on electrospun nanofibers decorated with ZnO nanorods and Ag nanoparticles for protective clothing applications. ACS Appl Mater Interfaces **13**(4), 5678–5690 (2021)
20. J.L. Frieiro, C. Guillaume, J. López-Vidrier, O. Blázquez, S. González-Torres, C. Labbé, S. Hernández, X. Portier, B. Garrido, Toward RGB LEDs based on rare earth-doped ZnO. Nanotechnol **31**(46), 465207 (2020)
21. N. Kaur, M. Singh, E. Comini, One-dimensional nanostructured oxide chemoresistive sensors. Langmuir. **36**(23), 6326–6344 (2020)
22. A. Marikutsa, M. Rumyantseva, E.A. Konstantinova, A. Gaskov, The key role of active sites in the development of selective metal oxide sensor materials. Sensors (Basel) **21**(7), 2554 (2021)
23. P. Nakarungsee, S. Srirattanapibul, C. Issro, I.M. Tang, S. Thongmee, High performance Cr doped ZnO by UV for NH_3 gas sensor. Sensors Actuators A Phys **314**, 112230 (2020)
24. M.M. Alam, A.M. Asiri, M.M. Rahman, Fabrication of phenylhydrazine sensor with V_2O_5 doped ZnO nanocomposites. Mater Chem Phys **243**, 122658 (2020)
25. S. Wang, F. Jia, X. Wang, L. Hu, Y. Sun, G. Yin, T. Zhou, Z. Feng, P. Kumar, B. Liu, Fabrication of ZnO nanoparticles modified by uniformly dispersed Ag nanoparticles: enhancement of gas sensing performance. ACS Omega **5**(10), 5209–5218 (2020)
26. Z. Wang, Z. Tian, D. Han, F. Gu, Au-modified three-dimensionally ordered macroporous ZnO: In for high-performance ethanol sensors. J Mater Chem C **8**, 2812–2819 (2020)
27. U. Godavarti, V.D. Mote, M. Dasari, Precipitated nickel doped ZnO nanoparticles with enhanced low temperature ethanol sensing properties. Mod Electron Mater **3**, 179–185 (2017)
28. R. Yoo, A.T. Güntner, Y. Park, H.J. Rim, H.S. Lee, W. Lee, Sensing of acetone by Al-doped ZnO. Sensors Actuators B Chem **283**, 107–115 (2019)
29. S. Ishak, S. Johari, M.M. Ramli, Influence of Sn dopant on ZnO thin film for formaldehyde detection. J Phys Conf Ser **1535**(012003), 012003 (2020)
30. S. Ishak, S. Johari, M.M. Ramli, Formaldehyde detection using Sn doped ZnO thin film. J Sol-Gel Sci Technol **95**, 265–275 (2020)
31. Q.A. Drmosh, I. Olanrewaju Alade, M. Qamar, S. Akbar, Zinc oxide-based acetone gas sensors for breath analysis: a review. Chem Asian J **16**, 1519–1538 (2021). https://doi.org/10.1002/asia.202100303
32. N.P. Shetti, S.D. Bukkitgar, K.R. Reddy, C.V. Reddy, T.M. Aminabhavi, ZnO-based nanostructured electrodes for electrochemical sensors and biosensors in biomedical applications. Biosens Bioelectron **141**, 111417 (2019)
33. S. Sagadevan, S. Vennila, S.N. Suraiya Begum, Y.A. Wahab, N. A.B. Hamizi, A.R. Marlinda, M.R. Johan, N. Ahmad, A. Umar, M. Ajmal Khan, H. Algarni, Influence of incorporated barium ion on the physio-chemical properties of zinc oxide nanodisks synthesized via a sonochemical process. J Nanosci Nanotechnol **20**(9), 5452–5457 (2020)
34. Y. Gu, G. Teng, X. Jin, L. Wang, Z. Qiang, W. Ma, C. Zhang, Shape-controlled synthesis of coral-like ZnO/C-$ZnFe_2O_4$ hierarchical structures and their improved photocatalytic antibacterial efficiency under visible light illumination. Ind Eng Chem Res **59**(24), 11219 (2020)
35. J.M. Ziegler, I. Andoni, E.J. Choi, L. Fang, H. Flores-Zuleta, N.J. Humphrey, D.H. Kim, J. Shin, H. Youn, R.M. Penner, Sensors based upon nanowires, nanotubes, and nanoribbons: 2016-2020. Anal Chem **93**(1), 124–166 (2021)
36. D. Commandeur, G. Brown, E. Hills, J. Spencer, Q. Chen, Defect-rich ZnO nanorod arrays for efficient solar water splitting. ACS Appl Nano Mater **2**(3), 1570–1578 (2019)
37. A. Galán-González, A.K. Sivan, J. Hernández-Ferrer, L. Bowen, L. Di Mario, F. Martelli, A.M. Benito, W.K. Maser, M.U. Chaudhry, A. Gallant, D.A. Zeze, D. Atkinson, Cobalt-doped ZnO nanorods coated with nanoscale metal-organic framework shells for water-splitting photoanodes. ACS Appl Nano Mater **3**(8), 7781–7788 (2020)
38. H. Li, M. Liu, J. Zhao, H. Gao, J. Feng, L. Jiang, Y. Wu, Controllable heterogeneous nucleation for patterning high-quality vertical and horizontal ZnO microstructures toward photodetectors. Small. **16**(42), e2004136 (2020)
39. Y. Wang, F. Zhong, H. Wang, H. Huang, Q. Li, J. Ye, M. Peng, T. He, Y. Chen, Y. Wang, L. Zhang, H. Zhu, X. Wang, Photogating-controlled ZnO photodetector response for visible to near-infrared light. Nanotechnology **31**(33), 335204 (2020)
40. Y.T. Tsai, S.J. Chang, L.W. Ji, Y.J. Hsiao, I.T. Tang, Fast detection and flexible microfluidic pH sensors based on Al-doped ZnO nanosheets with a novel morphology. ACS Omega **4**(22), 19847–19855 (2019)
41. C. Jin, W. Li, Y. Chen, R. Li, J. Huo, Q. He, Y. Wang, Efficient photocatalytic degradation and adsorption of tetracycline over type-II heterojunctions consisting of ZnO nanorods and K-doped exfoliated g-C_3N_4 nanosheets. Ind Eng Chem Res **59**(7), 2860–2873 (2020)
42. K. Zheng, H. Liu, C. Nie, X. Zhang, H. Hu, G. Ma, H. Wang, J. Huo, Controllable synthesis of honeycomb structured ZnO nanomaterials for photocatalytic degradation of methylene blue. Mater Lett **253**, 30–33 (2019)
43. S. Park, S.A. Moore, J. Lee, I.H. Song, B. Farshchian, N. Kim, Hydrothermal growth of ZnO nanowires on UV-nanoimprinted polymer structures. J Nanosci Nanotechnol **18**(5), 3686–3692 (2018)
44. H. Cao, Z. Liu, T. Liu, S. Duo, L. Huang, S. Yi, L. Cai, Well-organized assembly of ZnO hollow cages and their derived Ag/ZnO composites with enhanced photocatalytic property. Mater Charact **160**, 110125 (2020)
45. A.N. Kadam, D.P. Bhopate, V.V. Kondalkar, S.M. Majhi, C.D. Bathula, A.V. Tran, S.W. Lee, Facile synthesis of Ag-ZnO core–shell nanostructures with enhanced photocatalytic activity. J Ind Eng Chem **61**, 78–86 (2018)
46. B. Sarma, B.K. Sarma, Fabrication of Ag/ZnO heterostructure and the role of surface coverage of ZnO microrods by Ag nanoparticles on the photophysical and photocatalytic properties of the metal-semiconductor system. Appl Surf Sci **410**(557–565), 557–565 (2017)
47. S. Harish, J. Archana, M. Navaneethan, A. Silambarasan, K.D. Nisha, S. Ponnusamy, C. Muthamizhchelvan, H. Ikeda, D.K. Aswal, Y. Hayakawa, Enhanced visible light induced photocatalytic activity on the degradation of organic pollutants by SnO

nanoparticle decorated hierarchical ZnO nanostructures. RSC Adv **6**, 89721–89731 (2016)
48. C.-J. Chang, Y.-H. Wei, K.-P. Huang, Photocatalytic hydrogen production by flower-like graphene supported ZnS composite photocatalysts. Int J Hydrog Energy **42**, 23578–23586 (2017)
49. Y. Li, T. Liu, S. Feng, W. Yang, Y. Zhu, Y. Zhao, Z. Liu, H. Yang, W. Fu, Au/CdS Core-shell sensitized actinomorphic flower-like ZnO nanorods for enhanced photocatalytic water splitting performance. Nanomaterials (Basel) **11**(1), 233 (2021)
50. S. Sharma, D. Kumar, N. Khare, Hierarchical PANI/ZnO nanocomposite: synthesis and synergistic effect of shape selective ZnO nanoflowers and polyaniline sensitization for efficient photocatalytic dye degradation and photoelectrochemical water splitting. Nanotechnology **31**(46), 465402 (2020)
51. S.Z. Umbaidilah, N.A.M. Asib, A.N. Afaah, M. Rusop, Z. Khusaimi, A review on the effect of metal doped ZnO nanostructures on ultraviolet photoconductive sensor performance. AIP Conf Proc **2151**, 020038 (2019)
52. C.N. Wang, Y.L. Li, F.L. Gong, Y.H. Zhang, S.M. Fang, H.L. Zhang, Advances in doped ZnO nanostructures for gas sensor. Chem Rec **20**(12), 1553–1567 (2020)
53. I. Djerdi, Z. Jaglicic, D. Arcon, M. Niederberger, Co-Doped ZnO nanoparticles: minireview. Nanoscale. **2**, 1096–1104 (2010)
54. E. Ozugurlu, Cd-doped ZnO nanoparticles: an experimental and first principles DFT studies. J Alloys Compd **861**, 158620 (2021)
55. A.B. Patil, K.R. Patil, S.K. Pardeshi, Ecofriendly synthesis and solar photocatalytic activity of S-doped ZnO. J Hazard Mater **183**, 315–323 (2010)
56. J. Sowik, M. Miodyńska, B. Bajorowicz, A. Mikolajczyk, W. Lisowski, T. Klimczuk, D. Kaczor, A. Zaleska Medynska, A. Malankowska, Optical and photocatalytic properties of rare earth metal-modified ZnO quantum dots. Appl Surf Sci **464**, 651–663 (2019)
57. I.L. Poul Raj, S. Valanarasu, K. Hariprasad, J.S. Ponraj, N. Chidhambaram, V. Ganesh, H.E. Ali, Y. Khairy, Enhancement of optoelectronic parameters of Nd-doped ZnO nanowires for photodetector applications. Opt Mater (Amst) **109**(110396), 110396 (2020)
58. M. Kumar, K. Negi, A. Umar, M.S. Chauhan, Photocatalytic and fluorescent chemical sensing applications of La-doped ZnO nanoparticles. Chem Pap **75**, 1555–1566 (2020)
59. S. Anandan, A. Vinu, K.L.P. Sheeja Lovely, N. Gokulakrishnan, P. Srinivasu, T. Mori, V. Murugesan, V. Sivamurugan, K. Ariga, K (2007) Photocatalytic activity of La-doped ZnO for the degradation of monocrotophos in aqueous suspension. J Mol Catal A Chem **266**(149–157), 149–157 (2007)
60. T.L. Tan, C.W. Lai, S.B. Abd Hamid, Tunable band gap energy of Mn-doped ZnO nanoparticles using the coprecipitation technique. J Nanomater **2014**, 1–6 (**2014**). https://doi.org/10.1155/2014/371720
61. R. Viswanatha, S. Sapra, S. Sen Gupta, B. Satpati, P.V. Satyam, B.N. Dev, D.D. Sarma, Synthesis and characterization of Mn-doped ZnO nanocrystals. J Phys Chem B **108**, 6303–6310 (2004)
62. M. Long, H. Yuan, P. Sun, L. Su, X. Jiang, UV-assisted room temperature gas sensing with ZnO-Ag heterostructure nanocrystals studied by photoluminescence. J Nanosci Nanotechnol **21**(9), 4865–4869 (2021)
63. S. Sakthivel, B. Neppolian, M. Shankar, B. Arabindoo, M. Palanichamy, V. Murugesan, Solar photocatalytic degradation of azo dye: comparison of photocatalytic efficiency of ZnO and TiO_2. Sol Energy Mater Sol Cells **77**(1), 65–82 (2021)
64. B. Neppolian, H. Choi, S. Sakthivel, B. Arabindoo, V. Murugesan, Solar/UV-induced photocatalytic degradation of three commercial textile dyes. J Hazard Mater **89**, 303–317 (2002)
65. R. Saleh, N.F. Djaja, Transition-metal-doped ZnO nanoparticles: synthesis, characterization and photocatalytic activity under UV light. Spectrochim Acta A Mol Biomol Spectrosc **130**, 581–590 (2014)
66. B. Neppolian, S. Sakthivel, B. Arabindoo, M. Palanichamy, V. Murugesan, Degradation of textile dye by solar light using TiO_2 and ZnO photocatalysts. J Environ Sci Health A **34**, 1829–1838 (1999)
67. Ü. Özgür, Y.I. Alivov, C. Liu, A. Teke, M. Reshchikov, S. Doğan, V.C.S.J. Avrutin, S.J. Cho, A.H. Morkoç, A comprehensive review of ZnO materials and devices. J Appl Phys **98, 11**(4) (2005)
68. T.C.Z.K. Ellmer, A. Klein, B. Rech, Mater Sci Forum **104** (2008)
69. W. Gao, Z. Li, ZnO thin films produced by magnetron sputtering. Ceram Int **30**, 1155–1159 (2004)
70. D. Ramírez, K. Álvarez, G. Riveros, M. Tejos, M. Lobos, New insights on the doping of ZnO films with elements from group IIIA through electrochemical deposition. J Solid State Electrochem **18**, 2869–2884 (2014)
71. A. K. Das, P. Misra, R. Ajimsha, D. Phase, L. Kukreja, Metal to semiconductor transition in lightly Al doped ZnO thin films grown by sequential pulsed laser deposition, Laser Materials Processsing Division, Raja Ramanna Center for Advanced Technology, Indore–452. 13 www.arxiv.org
72. Y. Wang, H. Wang, Y. Wang, W. Ding, S. Peng, W. Chai, Preparation and properties of surface textured ZnO: Al films by direct current pulse magnetron sputtering. J Mater Sci Mater Electron **24**, 53–57 (2013)
73. H.J. Lee, J.H. Kim, S.S. Park, S.S. Hong, G.D. Lee, Degradation kinetics for photocatalytic reaction of methyl orange over Al-doped ZnO nanoparticles. J Ind Eng Chem **25**, 199–206 (2015)
74. M. Ahmad, E. Ahmed, Y. Zhang, N.R. Khalid, J. Xu, M. Ullah, Z. Hong, Preparation of highly efficient Al-doped ZnO photocatalyst by combustion synthesis. Curr Appl Phys **13**, 697–704 (2013)
75. F. Maldonado, A. Stashans, Al-doped ZnO: Electronic, electrical and structural properties. J Phys Chem Solids **71**, 784–787 (2010)
76. Y. Yang, J. Qi, Q. Liao, Y. Zhang, X. Yan, Y. Huang, L. Tang, Fabrication, structural characterization, and photoluminescence of Ga-doped ZnO nanobelts. Appl Phys A Mater Sci Process **94**, 799–803 (2009)
77. S. Kuprenaite, T. Murauskas, A. Abrutis, V. Kubilius, Z. Saltyte, V. Plausinaitiene, Properties of In, Ga-, and Al-doped ZnO films grown by aerosol-assisted MOCVD: Influence of deposition temperature, doping level and annealing. Surf Coat Technol **271**, 156–164 (2015)
78. L. Xu, Y. Su, Y. Chen, H. Xiao, L.A. Zhu, Q. Zhou, S. Li, Synthesis and characterization of indium-doped ZnO nanowires with periodical single− twin structures. J Phys Chem B **110**, 6637–6642 (2006)
79. C.H. Tan, S.T. Tan, H.B. Lee, R.T. Ginting, H.F. Oleiwi, C.C. Yap, M.H.H. Jumali, M. Yahaya, Automated room temperature optical absorbance CO sensor based on In-doped ZnO nanorod. Sensors Actuators B Chem **248**(140-152), 140–152 (2017)
80. M.R. Prasad, M. Haris, M. Sridharan, Investigation on structural, morphological, optical and ammonia sensing properties indium doped nano crystalline ZnO thin films synthesized by spray pyrolysis technique. Sensing and Imaging **19**, 1–14 (2018)
81. P.R. Kumar, C.S. Kartha, K. Vijayakumar, et al., On the properties of indium doped ZnO thin films. Semicond Sci Technol **20**, 120 (2004)
82. F. Zahedi, R. Dariani, S. Rozati, Structural, optical and electrical properties of ZnO thin films prepared by spray pyrolysis: effect of precursor concentration. Bull Mater Sci **37**, 433–439 (2014)
83. S. Bharath, K.V. Bangera, G. Shivakumar, Enhanced gas sensing properties of indium doped ZnO thin films. Superlattice Microst **124**, 72–78 (2018)

84. C.H. Ahn, H. Kim, H.K. Cho, Deposition of Al doped ZnO layers with various electrical types by atomic layer deposition. Thin Solid Films **519**, 747–750 (2010)
85. B. Sahoo, D. Behera, S.K. Pradhan, et al., Analysis of structural, optical and electrical properties of nano-particulate indium doped zinc oxide thin films. Mater Res Express **6**, 1150a1156 (2019)
86. S.Y. Bae, H.C. Choi, C.W. Na, J. Park, Influence of incorporation on the electronic structure of ZnO nanowires. Appl Phys Lett **86**, 033102 (2005)
87. L. Peng, L. Hu, X. Fang, Low-dimensional nanostructure ultraviolet photodetectors. Adv Mater **25**, 5321–5328 (2013)
88. H. Sato, T. Minami, S. Takata, Highly transparent and conductive group IV impurity-doped ZnO thin films prepared by radio frequency magnetron sputtering. J Vac Sci Technol **11**(6), 2975–2979 (1993)
89. H. Sato, T. Minami, E. Yamada, M. Ishii, S. Takata, Transparent and conductive impurity-doped GaN thin films prepared by an electron cyclotron resonance plasma metalorganic chemical vapor deposition method. J Appl Physiol **75**, 1405–1409 (1994)
90. H. Nanto, T. Minami, S. Shooji, S. Takata, Electrical and optical properties of zinc oxide thin films prepared by rf magnetron sputtering for transparent electrode applications. J Appl Physiol **55**, 1029–1034 (1984)
91. H. Benelmadjat, B. Boudine, A. Keffous, N. Gabouze, Photoresponse and H2 gas sensing properties of highly oriented Al and Al/Sb doped ZnO thin films. Progress in Natural Science: Materials International **23**, 519–523 (2013)
92. R. Saha, A. Karmakar, S. Chattopadhyay, Comparative investigation of Ga-and Sn-doped ZnO nanowires/p-Si heterojunctions for UV-photo sensing, Proccedings of Conference Comparative investigation of Ga-and Sn-doped ZnO nanowires/p-Si heterojunctions for UV-photo sensing, 1-5 (2018)
93. V. Ganesh, I. Yahia, S. AlFaify, M. Shkir, Sn-doped ZnO nanocrystalline thin films with enhanced linear and nonlinear optical properties for optoelectronic applications. J Phys Chem Solids Physics and Chemistry of Solids **100**, 115–125 (2017)
94. S.T. Tan, B. Chen, X. Sun, et al., Blueshift of optical band gap in ZnO thin films grown by metal-organic chemical-vapor deposition. J Appl Physiol **98**, 013505 (2005)
95. Y. Liu, X. Chen, Y. Xu, Q. Zhang, X. Wang, Highly branched Sn-doped ZnO nanostructures for sunlight driven photocatalytic reactions. J Nanomater **2014**, 1–7 (**2014**)
96. M. Ahmad, C. Pan, W. Yan, J. Zhu, Effect of Pb-doping on the morphology, structural and optical properties of ZnO nanowires synthesized via modified thermal evaporation. Mater Sci Eng B **174**(55-58), 55–58 (2010)
97. D. Chu, Y.P. Zeng, D. Jiang, Hydrothermal synthesis and optical properties of Pb^{2+} doped ZnO nanorods. Mater Lett **60**, 2783–2785 (2006)
98. R. Yousefi, F. Jamali-Sheini, M. Cheraghizade, L. Zaman, Synthesis and characterization of Pb-doped ZnO nanoparticles and their photocatalytic applications. Mater Res Innov **20**, 121–127 (2016)
99. A. Boumaiza, B. Boudine, M. Sebais, Fabrication and characterization of pure and Pb-doped ZnO thin films prepared by sol–gel and dip-coating method. J Inorg Organomet Polym Mater, 1–6 (2021)
100. A.M.A. Ali, N.M. Ahmed, N.A. Kabir, S.M. Mohammad, Investigation on the characteristics of ZnO and ZnO-Pb structure for gamma radiation detection. Proccedings of Conference Investigation on the characteristics of ZnO and ZnO-Pb structure for gamma radiation detection **1535**, 012028 (2020)
101. N. Kannadasan, N. Shanmugam, S. Cholan, K. Sathishkumar, R. Poonguzhali, G. Viruthagiri, Synergistic effect of bimetal ions (Ce, Pb) incorporation on optical, structural, and sensory activity of ZnO nanocrystals. J Solid State Electrochem **19**, 757–768 (2015)
102. I.I. Valan, V. Gokulakrishnan, A. Stephen, K. Ramamurthi, Preparation and characterization of lead doped zinc oxide thin films. Proccedings of Conference Preparation and characterization of lead doped zinc oxide thin films **1512**, 662–663 (2013)
103. M. Sathya, K. Pushpanathan, Synthesis and optical properties of Pb doped ZnO nanoparticles. Appl Surf Sci **449**, 346–357 (2018)
104. A. Kashyout, H. Soliman, H. Shokry Hassan, A. Abousehly, Fabrication of ZnO and ZnO: Sb nanoparticles for gas sensor applications. J Nanomater **2010**, 1–8 (**2010**)
105. T. Aoki, Y. Hatanaka, D.C. Look, ZnO diode fabricated by excimer-laser doping. Appl Phys Lett **76**, 3257–3258 (2000)
106. K.C. Yung, H. Liem, H. Choy, Enhanced redshift of the optical band gap in Sn-doped ZnO free standing films using the sol–gel method. J Phys D Appl Phys **42**, 185002 (2009)
107. M. Olvera, A. Maldonado, R. Asomoza, ZnO: F thin films deposited by chemical spray: effect of the fluorine concentration in the starting solution. Sol Energy Mater Sol Cells **73**, 425–433 (2002)
108. Ö. Çelik, Ş. Baturay, Y.S. Ocak, Sb doping influence on structural properties of ZnO thin films. Mater Res Express **7**, 026403 (2020)
109. S. Mohite, K. Rajpure, Synthesis and characterization of Sb doped ZnO thin films for photodetector application. Opt Mater **36**, 833–838 (2014)
110. S. Jagadhesan, N. Senthilkumar, V. Senthilnathan, T. Senthil, Sb doped ZnO nanostructures prepared via co-precipitation approach for the enhancement of MB dye degradation. Mater Res Express **5**, 025040 (2018)
111. S.D. Baek, P. Biswas, J.-W. Kim, Y.C. Kim, T.I. Lee, J.-M. Myoung, Low-temperature facile synthesis of Sb-doped p-type ZnO nanodisks and its application in homojunction light-emitting diode. ACS Appl Mater Interfaces **8**, 13018–13026 (2016)
112. H. Benelmadjat, B. Boudine, O. Halimi, M. Sebais, Fabrication and characterization of pure and Sn/Sb-doped ZnO thin films deposited by sol–gel method. Opt Laser Technol **41**, 630–633 (2009)
113. L. Mandalapu, F. Xiu, Z. Yang, D. Zhao, J. Liu, p-type behavior from Sb-doped ZnO heterojunction photodiodes. Appl Phys Lett **88**, 112108 (2006)
114. V. Chandraboss, L. Natanapatham, B. Karthikeyan, J. Kamalakkannan, S. Prabha, S. Senthilvelan, Effect of bismuth doping on the ZnO nanocomposite material and study of its photocatalytic activity under UV-light. Mater Res Bull **48**, 3707–3712 (2013)
115. Z. Xu, Y. Liu, W. Zhou, M.O. Tade, Z. Shao, B-site cation-ordered double-perovskite oxide as an outstanding electrode material for supercapacitive energy storage based on the anion intercalation mechanism. ACS Appl Mater Interfaces **10**, 9415–9423 (2018)
116. C. Jain, R.L.M. Rodriguez, A.M. Phillippy, K.T. Konstantinidis, S. Aluru, High throughput ANI analysis of 90K prokaryotic genomes reveals clear species boundaries. Nat Commun **9**, 1–8 (2018)
117. R. Mastan, A.K. Zak, R.P. Shahri, Bi-doped ZnO yellow nanopigments: synthesis, characterization, and antibacterial application for painting humid places. Ceram Int **46**, 8582–8587 (2020)
118. S.S. Zahirullah, P. Immanuel, S. Pravinraj, P.F.H. Inbaraj, J.J. Prince, Synthesis and characterization of Bi doped ZnO thin films using SILAR method for ethanol sensor. Mater Lett **230**, 1–4 (2018)
119. B. Karthikeyan, C.S. Sandeep, R. Philip, M. Baesso, Study of optical properties and effective three-photon absorption in Bi-doped ZnO nanoparticles. J Appl Phys **106**, 114304 (2009)

120. E. F. Keşkenler, S. Aydın, G. Turgut, S. Doğan, Optical and structural properties of bismuth doped ZnO thin films by sol-gel method: urbach rule as a function of crystal defects. 2014
121. J. Kazmi, P.C. Ooi, B.T. Goh, M.K. Lee, M.F.M. Razip Wee, S. Shafura A Karim, S.R. Ali Raza, M.A. Mohamed, Bi-doping improves the magnetic properties of zinc oxide nanowires. RSC Adv **10**, 23297–23311 (2020)
122. A. Ghosh, N. Kumari, A. Bhattacharjee, Investigations on structural and optical properties of Cu doped ZnO. J Nanosci Nanotechnol **2**, 485–489 (2014)
123. P. Bandyopadhyay, A. Dey, R. Basu, S. Das, P. Nandy, Synthesis and characterization of copper doped zinc oxide nanoparticles and its application in energy conversion. Curr Appl Phys **14**, 1149–1155 (2014)
124. M. Chakraborty, A. Ghosh, R. Thangavel, Experimental and theoretical investigations of structural and optical properties of copper doped ZnO nanorods. J Sol-Gel Sci Techn **74**, 756–764 (2015)
125. Z. Ma, F. Ren, X. Ming, Y. Long, A.A. Volinsky, Cu-doped ZnO electronic structure and optical properties studied by first-principles calculations and experiments. Materials. **12**, 196 (2019)
126. O. Slimi, D. Djouadi, L. Hammiche, A. Chelouche, T. Touam, Structural and optical properties of Cu doped ZnO aerogels synthesized in supercritical ethanol. J Porous Mater **25**, 595–601 (2018)
127. M. Fang, C. Tang, Z. Liu, Microwave-assisted hydrothermal synthesis of Cu-doped ZnO single crystal nanoparticles with modified photoluminescence and confirmed ferromagnetism. J Electron Mater **47**, 1390–1396 (2018)
128. B.K. Das, T. Das, K. Parashar, A. Thirumurugan, S. Parashar, Structural, bandgap tuning and electrical properties of Cu doped ZnO nanoparticles synthesized by mechanical alloying. J Mater Sci Mater Electron **28**, 15127–15134 (2017)
129. C. Xia, F. Wang, C. Hu, Theoretical and experimental studies on electronic structure and optical properties of Cu-doped ZnO. J Alloys Compd **589**, 604–608 (2014)
130. A. Vanaja, M. Suresh, J. Jeevanandam, et al., Copper-doped zinc oxide nanoparticles for the fabrication of white LEDs. Prot Met Phys Chem Surf **55**, 481–486 (2019)
131. Y. Xu, B. Yao, Y. Li, et al., Chemical states of gold doped in ZnO films and its effect on electrical and optical properties. J Alloys Compd **585**, 479–484 (2014)
132. Y. Yan, M. Al-Jassim, S.-H. Wei, Doping of ZnO by group-IB elements. Appl Phys Lett **89**, 181912 (2006)
133. P. Georgiev, N. Kaneva, A. Bojinova, K. Papazova, K. Mircheva, K. Balashev, Effect of gold nanoparticles on the photocatalytic efficiency of ZnO films. Colloid Surf A-Physicochem Eng Asp **460**, 240–247 (2014)
134. M. Deshwal, A. Arora, Enhanced acetone detection using Au doped ZnO thin film sensor. J Mater Sci Mater Electron **29**, 15315–15320 (2018)
135. L. Ouarez, A. Chelouche, T. Touam, R. Mahiou, D. Djouadi, A. Potdevin, Au-doped ZnO sol-gel thin films: an experimental investigation on physical and photoluminescence properties. J Lumin **203**, 222–229 (2018)
136. S. Baruah, B. Maibam, C. K. Borah, T. Agarkar, A. Kumar, S. Kumar, A Highly receptive ZnO based enzymatic electrochemical sensor for glucose sensing, IEEE Sensors Journal. 2021
137. M. Mamat, M. Sahdan, Z. Khusaimi, A. Zain, Z. Ahmed, S. Abdullah, M. Rusop, Influence of doping concentrations on the aluminum doped zinc oxide thin films properties for ultraviolet photoconductive sensor applications. Opt Mater(Amst) **32**, 696–699 (2010)
138. H. Wang, L. Xu, J. Fan, et al, Study of solid solubility of gold doped in ZnO films and its effect on optical properties, Proccedings of Conference Study of solid solubility of gold doped in ZnO films and its effect on optical properties, 407-410 (2015)
139. G. Venugopal, S. Thangavel, V. Vasudevan, K. Zoltán, Efficient visible-light piezophototronic activity of ZnO-Ag8S hybrid for degradation of organic dye molecule. J Phys Chem Solids **143**, 109473 (2020)
140. A. Chauhan, R. Verma, S. Kumari, et al., Photocatalytic dye degradation and antimicrobial activities of pure and Ag-doped ZnO using Cannabis sativa leaf extract. Sci Rep **10**, 1–16 (2020)
141. R. Rajendran, A. Mani, Photocatalytic, antibacterial and anticancer activity of silver-doped zinc oxide nanoparticles. J Saudi Chem Soc **24**, 1010–1024 (2020)
142. D. Thakur, A. Sharma, D.S. Rana, N. Thakur, D. Singh, T. Tamulevicius, M. Andrulevicius, S. Tamulevicius, S.K. Shukla, S. Thakur, Facile synthesis of silver-doped zinc oxide nanostructures as efficient scaffolds for detection of p-Nitrophenol. Chemosensors. **8**, 108 (2020)
143. I. Ahmad, E. Ahmed, M. Ahmad, The excellent photocatalytic performances of silver doped ZnO nanoparticles for hydrogen evolution. SN Applied Sciences **1**, 1–12 (2019)
144. I. Ahmad, E. Ahmed, M. Ullah, et al., Synthesis and characterization of silver doped ZnO nanoparticles for hydrogen production. J Ovonic Res **14** (2018)
145. S. Li, Z. Ma, J. Zhang, Y. Wu, Y. Gong, A comparative study of photocatalytic degradation of phenol of TiO_2 and ZnO in the presence of manganese dioxides. Catal Today **139**, 109–112 (2008)
146. A. Saboor, S.M. Shah, H. Hussain, Band gap tuning and applications of ZnO nanorods in hybrid solar cell: Ag-doped verses Nd-doped ZnO nanorods. Mater Sci Semicond Process **93**, 215–225 (2019)
147. Y. Zhang, Z. Zhang, B. Lin, Z. Fu, J. Xu, Effects of Ag doping on the photoluminescence of ZnO films grown on Si substrates. J Phys Chem B **109**, 19200–19203 (2005)
148. C. Karunakaran, A. Vijayabalan, G. Manikandan, Photocatalytic and bactericidal activities of hydrothermally synthesized nanocrystalline Cd-doped ZnO. Superlattice Microst **51**, 443–453 (2012)
149. S. Mondal, P. Mitra, Preparation of cadmium-doped ZnO thin films by SILAR and their characterization. Bull Mater Sci **35**, 751–757 (2012)
150. J. Li, M. Ren, J. Qing, Y. Wang, Z. Liang, N. Wang, J. Tong, C. Yang, Y. Xia, Solution-processible Cd-doped ZnO nanoparticles as an electron transport layer to achieve high performance polymer solar cells through improve conductivity and light transmittance. Mol Cryst Liq Cryst **692**, 74–82 (2019)
151. K.P. Ghoderao, S.N. Jamble, R.B. Kale, Hydrothermally synthesized Cd-doped ZnO nanostructures with efficient sunlight-driven photocatalytic and antibacterial activity. J Mater Sci Mater Electron **30**, 11208–11219 (2019)
152. A. Phuruangrat, S. Mad-ahin, O. Yayapao, S. Thongtem, T. Thongtem, Photocatalytic degradation of organic dyes by UV light, catalyzed by nanostructured Cd-doped ZnO synthesized by a sonochemical method. Res Chem Intermed **41**, 9757–9772 (2015)
153. A. Mitrushchenkov, R. Linguerri, G. Chambaud, Piezoelectric Properties of AlN, ZnO, and Hg x Zn1− x O nanowires by first-principles calculations. J Phys Chem C **113**, 6883–6886 (2009)
154. R. Saravanan, M. Kumaresan, A. Stephen, T. Prakash, V. Narayanan, Preparation and characterization of Hg doped ZnO nanorods, Proccedings of Conference Preparation and characterization of Hg doped ZnO nanorods, 238-240 (2011)
155. R. Saravanan, V. Gupta, T. Prakash, V. Narayanan, A. Stephen, Synthesis, characterization and photocatalytic activity of novel Hg doped ZnO nanorods prepared by thermal decomposition method. J Mol Liq **178**, 88–93 (2013)
156. P. Mani, S.V. Nair, M. Shanmugam, Thickness-dependent hole-blocking capability of RF-sputtered nickel oxide compact layers in dye-sensitized solar cells. Emergent Materials **3**, 117–124 (2020)

157. P. Karthik, A. Pandikumar, M. Preeyanghaa, M. Kowsalya, B. Neppolian, Amino-functionalized MIL-101 (Fe) metal-organic framework as a viable fluorescent probe for nitroaromatic compounds. Microchim Acta **184**, 2265–2273 (2017)
158. S.V. Bhat, F. Deepak, Tuning the bandgap of ZnO by substitution with Mn^{2+}, Co^{2+} and Ni^{2+}. Solid State Commun **135**, 345–347 (2005)
159. D. Toloman, A. Mesaros, A. Popa, O. Raita, T.D. Silipas, B.S. Vasile, O. Pana, L.M. Giurgiu, Evidence by EPR of ferromagnetic phase in Mn-doped ZnO nanoparticles annealed at different temperatures. J Alloys Compd **551**, 502–507 (2013)
160. A. Iqbal, A. Mahmood, T.M. Khan, E. Ahmed, Structural and optical properties of Cr doped ZnO crystalline thin films deposited by reactive electron beam evaporation technique. Progress in Natural Science: Materials International **23**, 64–69 (2013)
161. R. Joshi, P. Kumar, A. Gaur, K. Asokan, Structural, optical and ferroelectric properties of V doped ZnO. Appl Nanosci **4**, 531–536 (2014)
162. O. Bayram, E. Sener, E. İgman, O. Simsek, Investigation of structural, morphological and optical properties of nickel-doped zinc oxide thin films fabricated by co-sputtering. J Mater Sci Mater Electron **30**, 3452–3458 (2019)
163. T. Hammad, J. Salem, R. Harrison, Structure, optical properties and synthesis of Co-doped ZnO superstructures Appl. Nanosci. **3**, 133–139 (2013)
164. V. Gandhi, R. Ganesan, H.H.A.S. Hamed, M. Thaiyan, Effect of cobalt doping on structural, optical, and magnetic properties of ZnO nanoparticles synthesized by coprecipitation method. J Phys Chem C **118**, 9715–9725 (2014)
165. N.-E. Sung, K.-S. Lee, I.-J. Lee, Structural characterization of Zr-doped ZnO films deposited on quartz substrates by reactive radio frequency magnetron co-sputtering. Thin Solid Films **651**, 42–47 (2018)
166. T. Srinivasulu, K. Saritha, K.R. Reddy, Synthesis and characterization of Fe-doped ZnO thin films deposited by chemical spray pyrolysis. Mod Electron Mater **3**, 76–85 (2017)
167. E. Aslan, M. Zarbali, Highly sensitive zinc oxide ultraviolet photodetector by titanium incorporation. Thin Solid Films **724**, 138627 (2021)
168. N. Shakti, C. Devi, A. Patra, P. Gupta, S. Kumar, Lithium doping and photoluminescence properties of ZnO nanorods. AIP Adv **8**, 015306 (2018)
169. J. Lander, Reactions of Lithium as a donor and an acceptor in ZnO. J Phys Chem Solids **15**, 324–334 (1960)
170. P. Manzhi, M.B. Alam, R. Kumari, R. Krishna, R.K. Singh, R. Srivastava, O.P. Sinha, Li-doped ZnO nanostructures for the organic light emitting diode application. Vacuum. **146**, 462–467 (2017)
171. A. Soultati, A. Fakharuddin, E. Polydorou, C. Drivas, A. Kaltzoglou, M.I. Haider, F. Kournoutas, M. Fakis, L.C. Palilis, S. Kennou, D. Davazoglou, P. Falaras, P. Argitis, S. Gardelis, A. Kordatos, A. Chroneos, L. Schmidt-Mende, M. Vasilopoulou, Lithium doping of ZnO for high efficiency and stability fullerene and non-fullerene organic solar cells. ACS Appl Energy Mater **2**, 1663–1675 (2019)
172. M. Ardyanian, N. Sedigh, Heavy lithium-doped ZnO thin films prepared by spray pyrolysis method. Bull Mater Sci **37**, 1309–1314 (2014)
173. V. Bilgin, Preparation and characterization of ultrasonically sprayed zinc oxide thin films doped with lithium. J Electron Mater **38**, 1969–1978 (2009)
174. V. Srikant, D. Clarke, Anomalous behavior of the optical band gap of nanocrystalline zinc oxide thin films. J Mater Res **12**, 1425–1428 (1997)
175. G.A. Mohamed, E.-M. Mohamed, A.A. El-Fadl, Optical properties and surface morphology of Li-doped ZnO thin films deposited on different substrates by DC magnetron sputtering method. Phys Rev B Condens Matter **308**, 949–953 (2001)
176. W. Bin, Z. Yue, M. Jiahua, S. Wenbin, Ag–N dual-accept doping for the fabrication of p-type ZnO. Appl Phys A Mater Sci Process **94**, 715–718 (2009)
177. M. Chen, Y. Zhu, A. Chen, Z. Shen, Z. Tang, Optical investigations of Be doped ZnO films grown by molecular beam epitaxy. Mater Res Bull **78**, 16–19 (2016)
178. S.R. Thomas, G. Adamopoulos, T.D. Anthopoulos, Be-doped ZnO thin-film transistors and circuits fabricated by spray pyrolysis in air. J Disp Technol **9**, 688–693 (2012)
179. S. Ding, G. Fan, S. Li, K. Chen, B. Xiao, Theoretical study of BexZn1-xO alloys. Phys Rev B Condens Matter **394**, 127–131 (2007)
180. Y. Ryu, T. Lee, J. Lubguban, et al., Wide-band gap oxide alloy: BeZnO. Appl Phys Lett **88**, 052103 (2006)
181. J. Yu, D. Park, J. Kim, T. Jeong, C. Youn, K. Hong, Post-growth annealing and wide bandgap modulation of BeZnO layers grown by RF co-sputtering of ZnO and Be targets. J Mater Sci **45**, 130–135 (2010)
182. X. Fan, Z. Zhu, Y.-S. Ong, Y. Lu, Z. Shen, J.-L. Kuo, A direct first principles study on the structure and electronic properties of Be x Zn 1− x O. Appl Phys Lett **91**, 121121 (2007)
183. F. Kong, H. Gong, Influence of interstitial beryllium on properties of ZnO: A first-principle research. Comput Mater Sci **61**, 127–133 (2012)
184. D. Ye, Z. Mei, H. Liang, Y. Liu, A. Azarov, A. Kuznetsov, X. du, Beryllium sites in MBE-grown BeZnO alloy films. J Phys D Appl Phys **47**, 175102 (2014)
185. A. Chen, H. Zhu, Y. Wu, M. Chen, Y. Zhu, X. Gui, Z. Tang, Beryllium-Assisted p-type doping for ZnO homojunction light-emitting devices. Adv Funct Mater **26**, 3696–3702 (2016)
186. J.-K. Chung, W.-J. Kim, S.S. Kim, T.K. Song, C.J. Kim, Structural and optical properties of Be-doped ZnO nanocrystalline films by pulsed laser deposition. Thin Solid Films **516**, 4190–4193 (2008)
187. A.B. Patil, K.R. Patil, S.K. Pardeshi, Enhancement of oxygen vacancies and solar photocatalytic activity of zinc oxide by incorporation of nonmetal. J Solid State Chem **184**, 3273–3279 (2011)
188. R. Marschall, L. Wang, Non-metal doping of transition metal oxides for visible-light photocatalysis. Catal Today **225**, 111–135 (2014)
189. P. Mani, Y. Kim, S.K. Lakhera, B. Neppolian, H. Choi, Complete arsenite removal from groundwater by UV activated potassium persulfate and iron oxide impregnated granular activated carbon. Chemosphere. **277**, 130225 (2021)
190. V. Vinesh, A. Shaheer, B. Neppolian, Reduced graphene oxide (rGO) supported electron deficient B-doped TiO_2 (Au/B-TiO_2/rGO) nanocomposite: an efficient visible light sonophotocatalyst for the degradation of Tetracycline (TC). Ultrason Sonochem **50**, 302–310 (2019)
191. C.-Y. Tsay, W.-T. Hsu, Sol–gel derived undoped and boron-doped ZnO semiconductor thin films: preparation and characterization. Ceram Int **39**, 7425–7432 (2013)
192. B. Houng, C.-L. Huang, S.-Y. Tsai, Effect of the pH on the growth and properties of sol–gel derived boron-doped ZnO transparent conducting thin film. J Cryst Growth **307**, 328–333 (2007)
193. S. Kim, H. Yoon, S.-O. Kim, J.-Y. Leem, Optical properties and electrical resistivity of boron-doped ZnO thin films grown by sol–gel dip-coating method. Opt Mater **35**, 2418–2424 (2013)
194. V. Kumar, R. Singh, L. Purohit, R. Mehra, Structural, transport and optical properties of boron-doped zinc oxide nanocrystalline. J Mater Sci Technol **27**, 481–488 (2011)
195. Z.N. Kayani, Z. Bashir, S. Riaz, S. Naseem, Z. Saddiqe, Transparent boron-doped zinc oxide films for antibacterial and

magnetic applications. J Mater Sci Mater Electron **31**, 11911–11926 (2020)
196. C. Ballif, S. Fay, S. Myong, R. Schluchter, J. Steinhauser, E. Vallat, Boron doping effects on the electro-optical properties of zinc oxide thin films deposited by low-pressure chemical vapor deposition process. Proccedings of Conference Boron Doping Effects on the Electro-Optical Properties of Zinc Oxide Thin Films Deposited by Low-Pressure Chemical Vapor Deposition Process **928**, 98 (2006)
197. S. Bhattacharjee, M. Basu, A. Roy, Optical and electrical properties of undoped and boron doped zinc oxide synthesized by chemical route. Proccedings of Conference Optical and electrical properties of undoped and boron doped zinc oxide synthesized by chemical route **1675**, 020007 (2015)
198. W. Wang, T. Ai, Q. Yu, Electrical and photocatalytic properties of boron-doped ZnO nanostructure grown on PET–ITO flexible substrates by hydrothermal method. Sci Rep **7**, 1–11 (2017)
199. K. Edalati, A. Shakiba, J. Vahdati-Khaki, S.M. Zebarjad, Low-temperature hydrothermal synthesis of ZnO nanorods: effects of zinc salt concentration, various solvents and alkaline mineralizers. Mater Res Bull **74**, 374–379 (2016)
200. R.B.H. Tahar, N.B.H. Tahar, Boron-doped zinc oxide thin films prepared by sol-gel technique. J Mater Sci **40**, 5285–5289 (2005)
201. A. Tumbul, F. Aslan, S. Demirozu, et al., Solution processed boron doped ZnO thin films: influence of different boron complexes. Mater Res Bull **6**, 035903 (2018)
202. V. Vinesh, M. Ashokkumar, B. Neppolian, rGO supported self-assembly of 2D nano sheet of (g-C_3N_4) into rod-like nano structure and its application in sonophotocatalytic degradation of an antibiotic. Ultrason Sonochem **68**, 105218 (2020)
203. J.W. Park, D.H. Kim, S.H. Choi, M. Lee, D. Lim, The role of carbon doping in ZnO. J Korean Phys Soc **57**, 1482–1485 (2010)
204. J.J. Beltrán, C.A. Barrero, A. Punnoose, Relationship between ferromagnetism and formation of complex carbon bonds in carbon doped ZnO powders. Phys Chem Chem Phys **21**, 8808–8819 (2019)
205. L. Ntozakhe, R. T. Taziwa, Pyrolysis of carbon-doped ZnO nanoparticles for solar cell application. In Zinc Oxide Based Nano Materials and Devices). IntechOpen, (2019)
206. D.E. Zhang, M.Y. Wang, J.J. Ma, et al., Enhanced photocatalytic ability from carbon-doped ZnO photocatalyst synthesized without an external carbon precursor, Functional Mater. Lett. **7**, 1450026 (2014)
207. F. Cesano, D. Scarano, S. Bertarione, F. Bonino, A. Damin, S. Bordiga, C. Prestipino, C. Lamberti, A. Zecchina, Synthesis of ZnO–carbon composites and imprinted carbon by the pyrolysis of $ZnCl_2$-catalyzed furfuryl alcohol polymers. J Photochem Photobiol A **196**, 143–153 (2008)
208. C.C. Chenot, R.L. Robiette, S. Collin, First evidence of the cysteine and glutathione conjugates of 3-sulfanylpentan-1-ol in hop (Humulus lupulus L.). J Agric Food Chem **67**, 4002–4010 (2019)
209. S. Cho, J.-W. Jang, J.S. Lee, K.-H. Lee, Carbon-doped ZnO nanostructures synthesized using vitamin C for visible light photocatalysis. Cryst Eng Comm **12**, 3929–3935 (2010)
210. A. Lavand, Y. Malghe, Synthesis, characterization, and visible light photocatalytic activity of nanosized carbon doped zinc oxide. J Photochem Photobiol **2015** (**2015**)
211. S.A. Ansari, S. Ansari, H. Foaud, M.H. Cho, Facile and sustainable synthesis of carbon-doped ZnO nanostructures towards the superior visible light photocatalytic performance. New J Chem **41**, 9314–9320 (2017)
212. F. Wang, L. Liang, L. Shi, M. Liu, J. Sun, CO_2-assisted synthesis of mesoporous carbon/C-doped ZnO composites for enhanced photocatalytic performance under visible light. Dalton Trans **43**, 16441–16449 (2014)
213. H.-C. Wu, Y.-C. Peng, T.-P. Shen, Electronic and optical properties of substitutional and interstitial Si-doped ZnO. Materials. **5**, 2088–2100 (2012)
214. J. Zhao, L. Qin, L. Zhang, Synthesis of quasi-aligned Si-doped ZnO nanorods on Si substrate. Physica E: Low-dimensional Systems and Nanostructures **40**, 795–799 (2008)
215. R. Chowdhury, S. Adhikari, P. Rees, Optical properties of silicon doped ZnO. Phys B Condens Matter **405**, 4763–4767 (2010)
216. L. Besombes, D. Ferrand, H. Mariette, J. Cibert, M. Jamet, A. Barski, Spins in semiconducting nanostructures. Int J Nanotechnol **7**, 641–667 (2010)
217. D. Howard, P. Marchand, C. Carmalt, I. Parkin, J. Darr, Si-doped zinc oxide transparent conducting oxides; nanoparticle optimisation, scale-up and thin film deposition. J Mater Chem C **5**, 8796–8801 (2017)
218. Y. Wang, Z. Peng, Q. Wang, X. Fu, Tunable electrical resistivity of oxygen-deficient zinc oxide thin films. Surf Eng **33**, 217–225 (2017)
219. N. Rashidi, V.L. Kuznetsov, J.R. Dilworth, M. Pepper, P.J. Dobson, P.P. Edwards, Highly conducting and optically transparent Si-doped ZnO thin films prepared by spray pyrolysis. J Mater Chem C **1**, 6960–6969 (2013)
220. V.L. Kuznetsov, A.T. Vai, M. Al-Mamouri, J. Stuart Abell, M. Pepper, P.P. Edwards, Electronic transport in highly conducting Si-doped ZnO thin films prepared by pulsed laser deposition. Appl Phys Lett **107**, 232103 (2015)
221. H. Huang, G. Fang, X. Mo, L. Yuan, H. Zhou, M. Wang, H. Xiao, X. Zhao, Zero-biased near-ultraviolet and visible photodetector based on ZnO nanorods/n-Si heterojunction. Appl Phys Lett **94**, 063512 (2009)
222. T. Minami, H. Sato, H. Nanto, S. Takata, Highly conductive and transparent silicon doped zinc oxide thin films prepared by RF magnetron sputtering. Jpn J Appl Phys **25**, L776–L779 (1986)
223. J. Clatot, G. Campet, A. Zeinert, C. Labrugère, M. Nistor, A. Rougier, Low temperature Si doped ZnO thin films for transparent conducting oxides. Sol Energy Mater Sol Cells **95**, 2357–2362 (2011)
224. C. Park, S. Zhang, S.-H. Wei, Origin of p-type doping difficulty in ZnO: The impurity perspective. Phys Rev B **66**, 073202 (2002)
225. A. Kobayashi, O.F. Sankey, J.D. Dow, Deep energy levels of defects in the wurtzite semiconductors AIN, CdS, CdSe, ZnS, and ZnO. *Phys Rev* **28**, 946–956 (1983)
226. A. Boonchun, W.R. Lambrecht, Electronic structure of defects and doping in ZnO: Oxygen vacancy and nitrogen doping. Phys Status Solidi B **250**, 2091–2101 (2013)
227. W. Yu, J. Zhang, T. Peng, New insight into the enhanced photocatalytic activity of N-, C-and S-doped ZnO photocatalysts. Appl Catal B-Environ **181**, 220–227 (2016)
228. G. Kale, S. Arbuj, U. Kawade, S. Rane, J. Ambekar, B. Kale, Synthesis of porous nitrogen doped zinc oxide nanostructures using a novel paper mediated template method and their photocatalytic study for dye degradation under natural sunlight. Mater Chem Front **2**, 163–170 (2018)
229. R. Kumari, A. Sahai, N. Goswami, Effect of nitrogen doping on structural and optical properties of ZnO nanoparticles. Progress in Natural Science: Materials International **25**, 300–309 (2015)
230. Z.-N. Ng, K.-Y. Chan, S. Muslimin, D. Knipp, P-type characteristic of nitrogen-doped ZnO films. J Electron Mater **47**, 5607–5613 (2018)
231. J. Macías-Sánchez, L. Hinojosa-Reyes, A.D. Caballero-Quintero, et al., Synthesis of nitrogen-doped ZnO by sol–gel method: characterization and its application on visible photocatalytic degradation of 2, 4-D and picloram herbicides. Photochem Photobiol Sci **14**, 536–542 (2015)

232. R. Kabir, M. Saifullah, A. Khalid, et al., Synthesis of N-Doped ZnO nanocomposites for sunlight photocatalytic degradation of textile dye pollutants. J Compos Sci **4**, 49 (2020)
233. M. Hirai, A. Kumar, Effect of nitrogen doping on bonding state of ZnO thin films. J Vac Sci Technol **25**, 1534–1538 (2007)
234. H. Qin, W. Li, Y. Xia, T. He, Photocatalytic activity of heterostructures based on ZnO and N-doped ZnO. ACS Appl Mater Interfaces **3**, 3152–3156 (2011)
235. C. Gionco, D. Fabbri, P. Calza, M.C. Paganini, Synthesis, characterization, and photocatalytic tests of N-doped zinc oxide: a new interesting photocatalyst. J Nanomater **2016**, 1–7 (**2016**)
236. A. Allenic, W. Guo, Y. Chen, et al., Amphoteric phosphorus doping for stable p-Type ZnO. Adv Mater **19**, 3333–3337 (2007)
237. M.-P. Lu, J. Song, M.-Y. Lu, M.T. Chen, Y. Gao, L.J. Chen, Z.L. Wang, Piezoelectric nanogenerator using p-type ZnO nanowire arrays. Nano Lett **9**, 1223–1227 (2009)
238. Y. Heo, S. Park, K. Ip, S. Pearton, D. Norton, Transport properties of phosphorus-doped ZnO thin films. Appl Phys Lett **83**, 1128–1130 (2003)
239. W.-J. Lee, J. Kang, K.-J. Chang, Defect properties and p-type doping efficiency in phosphorus-doped ZnO. Phys Rev B **73**, 024117 (2006)
240. V. Siva, K. Park, M.S. Kim, et al., Mapping the structural, electrical, and optical properties of hydrothermally grown phosphorus-doped ZnO nanorods for optoelectronic device applications. Nanoscale Res Lett **14**, 1–9 (2019)
241. B. Panigrahy, D. Bahadur, P-type phosphorus doped ZnO nanostructures: an electrical, optical, and magnetic properties study. RSC Adv **2**, 6222–6227 (2012)
242. F. Shan, G. Liu, W. Lee, B. Shin, Stokes shift, blue shift and red shift of ZnO-based thin films deposited by pulsed-laser deposition. J Cryst Growth **291**, 328–333 (2006)
243. B. Panigrahy, M. Aslam, D.S. Misra, M. Ghosh, D. Bahadur, Defect-related emissions and magnetization properties of ZnO nanorods. Adv Funct Mater **20**, 1161–1165 (2010)
244. Y. Zhu, H. Yang, F. Sun, X. Wang, Controllable growth of ultrathin P-doped ZnO nanosheets. Nanoscale Res Lett **11**, 1–8 (2016)
245. J. Gao, Q. Zhao, Y. Sun, G. Li, J. Zhang, D. Yu, A novel way for synthesizing phosphorus-doped ZnO nanowires. Nanoscale Res Lett **6**, 1–6 (2011)
246. M. Mishra, S. Sushama, S.K. Pandey, S. Chakrabarti, Phosphorus doping of ZnO using spin-on dopant process: a better choice than costly and destructive ion-implantation technique. J Lumin **233**, 117921 (2021)
247. L.-C. Chen, Y.-J. Tu, Y.-S. Wang, R.-S. Kan, C.-M. Huang, Characterization and photoreactivity of N-, S-, and C-doped ZnO under UV and visible light illumination. J Photochem Photobiol A **199**, 170–178 (2008)
248. H. Zhang, Z. Tao, W. Xu, S. Lu, F. Yuan, First-principles study of dopants and defects in S-doped ZnO and its effect on photocatalytic activity. Comput Mater Sci **58**, 119–124 (2012)
249. X. Meng, Z. Shi, X. Chen, X. Zeng, Z. Fu, Temperature behavior of electron-acceptor transitions and oxygen vacancy recombinations in ZnO thin films. J Appl Phys **107**, 023501 (2010)
250. G. Shen, J.H. Cho, J.K. Yoo, G.-C. Yi, C.J. Lee, Synthesis and optical properties of S-doped ZnO nanostructures: nanonails and nanowires. J Phys Chem B **109**, 5491–5496 (2005)
251. J. Cho, Q. Lin, S. Yang, J.G. Simmons Jr., Y. Cheng, E. Lin, J. Yang, J.V. Foreman, H.O. Everitt, W. Yang, J. Kim, J. Liu, Sulfur-doped zinc oxide (ZnO) Nanostars: synthesis and simulation of growth mechanism. Nano Res **5**, 20–26 (2012)
252. B. Geng, G. Wang, Z. Jiang, et al., Synthesis and optical properties of S-doped ZnO nanowires. Appl Phys Lett **82**, 4791–4793 (2003)
253. W. Yu, J. Zhang, T. Peng, New insight into the enhanced photocatalytic activity of N-C-and S-doped ZnO photocatalysts. Applied Catalysis B: Environmental **181**, 220–227 (2016)
254. X.-Y. Xie, P. Zhan, L.-Y. Li, D.J. Zhou, D.Y. Guo, J.X. Meng, Y. Bai, W.J. Zheng, Synthesis of S-doped ZnO by the interaction of sulfur with zinc salt in PEG200. J Alloys Compd **644**, 383–389 (2015)
255. R.J. Ramalingam, A.K. Shukla, K. Kombaiah, J.J. Vijaya, A. Tawfeek, M. Synthesis, characterization and optical properties of sulfur and fluorine doped ZnO nanostructures for visible light utilized catalysis. Optik **148**, 325–331 (2017)
256. C. Platzer-Björkman, T. Törndahl, D. Abou-Ras, J. Malmström, J. Kessler, L. Stolt, Zn (O, S) buffer layers by atomic layer deposition in Cu (In, Ga) Se 2 based thin film solar cells: Band alignment and sulfur gradient. J Appl Phys **100**, 044506 (2006)
257. M. Jaquez, K. Yu, M. Ting, et al., Growth and characterization of ZnO1− xSx highly mismatched alloys over the entire composition. J Appl Phys **118**, 215702 (2015)
258. J.Z. Kong, H.F. Zhai, W. Zhang, S.S. Wang, X.R. Zhao, M. Li, H. Li, A.D. Li, D. Wu, Visible light-driven photocatalytic performance of N-Doped ZnO/g-C_3N_4 nanocomposites. Nanoscale Res Lett **12**(1), 526 (2017)
259. H.Y. Sohn, A. Murali, Plasma synthesis of advanced metal oxide nanoparticles and their applications as transparent conducting oxide thin films. Molecules **26**(5), 1456 (2021)
260. B.K. Singh, L. Agarwal, S. Tripathi, Fabrication and characterization of Cu doped ZnO/Bi doped ZnO nanolaminates as mirror for application in optical devices. IEEE Trans Nanotechnol **16**(2), 203–208 (2017)
261. S.G. Shin, J. Hur, H.W. Choi, A study on the characteristics of perovskite/ZnO-based ultraviolet sensors. J Nanosci Nanotechnol **21**(8), 4336–4340 (2021)
262. L. Qiaoping, L. Xin, Y. Yanning, Z. Fuchun, Z. Qi, Hydrothermal synthesis and optical properties of Fe doped ZnO nanorods. Ferroelectrics. **564**(1), 59–69 (2020)
263. M. Sabbaghan, M. Nadafan, H.R. Lamei, Cu-doped ZnO synthesis by ionothermal method: Morphology and optical properties. Opt Mater (Amst) **111**(110679), 110679 (2021)
264. A. Abraheem, Y. Abdulla, Preparation and characterization of the thermoluminescence properties of Mg-doped ZnO. Int J Sci Basic Appl Res **49**, 133–142 (2020)
265. C.H. Hsu, C.C. Lai, L.C. Chen, P.S. Chan, Enhanced performance of dye-sensitized solar cells with graphene/zno nanoparticles bilayer structure. J Nanomater **2014**(1), 1–6 (2014)
266. J. Bandara, K. Tennakone, P.P.B. Jayatilaka, Composite tin and zinc oxide nanocrystalline particles for enhanced charge separation in sensitized degradation of dyes. Chem. **49**(4), 439–445 (2002)
267. X. Xu, H. Zhang, J. Shi, J. Dong, Y. Luo, D. Li, Q. Meng, Highly efficient planar perovskite solar cells with a TiO_2/ZnO electron transport bilayer. J Mater Chem A **3**, 19288–19293 (2015)
268. A.E. Shalan, A.N. El-Shazly, M.M. Rashad, N.K. Allam, Tin-zinc-oxide nanocomposites (SZO) as promising electron transport layers for efficient and stable perovskite solar cells. Nanoscale Adv **1**, 2654–2662 (2019)
269. B.Y. Kadem, M.J. Mohammed Ali, A.F. Abdulameer, The effects of Al-doped ZnO layer on the performance of organic solar cell. Int Conf Dev Sys Eng (DeSE) **20**, 741–746 (2019)
270. N.E. Koksal, M. Sbeta, A. Atilgan, A. Yildiz, Al–Ga co-doped ZnO/Si heterojunction diodes. Phys B Condens Matter **600**(1), 412599 (2021)
271. S. Patial, R. Kumar, P. Raizada, P. Singh, Q. Van Le, E. Lichtfouse, D. Le Tri Nguyen, V.H. Nguyen, Boosting light-driven CO_2 reduction into solar fuels: mainstream avenues for engineering ZnO-based photocatalysts. Environ Res **197**, 111134 (2021)
272. M.M. Ba-Abbad, A.A.H. Kadhum, A.B. Mohamad, M.S. Takriff, K. Sopian, Visible light photocatalytic activity of Fe3+-doped

ZnO nanoparticle prepared via sol-gel technique. Chem. **91**(11), 1604–1611 (2013)
273. Z. Mirzaeifard, Z. Shariatinia, M. Jourshabani, S.M. Rezaei Darvishi, ZnO Photocatalyst revisited: effective photocatalytic degradation of emerging contaminants using S-doped ZnO nanoparticles under visible light radiation. Ind Eng Chem Res **59**(36), 15894–15911 (2020)
274. H. Lahmar, M. Benamira, S. Douafer, L. Messaadia, A. Boudjerda, M. Trari, Photocatalytic degradation of methyl orange on the novel hetero-system La_2NiO_4/ZnO under solar light. Chem Phys Lett **742**, 137132 (2020)
275. R. Saffari, Z. Shariatinia, M. Jourshabani, Synthesis and photocatalytic degradation activities of phosphorus containing ZnO microparticles under visible light irradiation for water treatment applications. Environ Pollut **259**, 113902 (2020)
276. N. Siva, D. Sakthi, S. Ragupathy, V. Arun, N. Kannadasan, Synthesis, structural, optical and photocatalytic behavior of Sn doped ZnO nanoparticles. Mater Sci Eng B **253**, 114497 (2020)
277. D. Dodoo-Arhin, T. Asiedu, B. Agyei-Tuffour, E. Nyankson, D. Obada, J.M. Mwabora, Photocatalytic degradation of Rhodamine dyes using zinc oxide nanoparticles. Mater Today Proc **38**(2), 809–815 (2021)
278. K.P. Raj, K. Sadaiyandi, A. Kennedy, S. Sagadevan, Z.Z. Chowdhury, M.R.J. Bin, F.A. Aziz, R.F. Rafique, R.T. Selvi, R. R. Bala, Influence of Mg doping on ZnO nanoparticles for enhanced photocatalytic evaluation and antibacterial analysis. Nanoscale Res Lett **13**, 229 (2018)
279. Y. Wang, X. Hao, Z. Wang, M. Dong, L. Cui, Facile fabrication of Mn^{2+}- doped ZnO photocatalysts by electrospinning. R Soc Open Sci **7**, 191050 (2020)
280. R.M. Mohamed, A.A. Ismail, M.W. Kadi, A.S. Alresheedi, I.A. Mkhalid, Photocatalytic performance mesoporous Nd_2O_3 modified ZnO nanoparticles with enhanced degradation of tetracycline. Catal Today (2020). https://doi.org/10.1016/j.cattod.2020.11.002
281. H. Pan, Y. Zhang, Y. Hu, H. Xie, Effect of cobalt doping on optical, magnetic and photocatalytic properties of ZnO nanoparticles. Optik (Stuttg) **208**(164560) (2020)
282. T.K. Pathak, E. Coetsee-Hugo, H.C. Swart, C.W. Swart, R.E. Kroon, Preparation and characterization of Ce doped ZnO nanomaterial for photocatalytic and biological applications. Mater Sci Eng B **261**, 114780 (2020)
283. M. Yarahmadi, H. Maleki-Ghaleh, M.E. Mehr, Z. Dargahi, F. Rasouli, M.H. Siadati, Synthesis and characterization of Sr-doped ZnO nanoparticles for photocatalytic applications. J Alloys Compd **853**, 157000 (2021)
284. R. Ahmad, S.M. Majhi, X. Zhang, T.M. Swager, K.N. Salama, Recent progress and perspectives of gas sensors based on vertically oriented ZnO nanomaterials. Adv Colloid Interf Sci **270**, 1–27 (2019)
285. M. Tomić, M. Šetka, L. Vojkůvka, S. Vallejos, VOCs Sensing by metal oxides, conductive polymers, and carbon-based materials. Nanomaterials **11**(2), 552 (2021)
286. F. Vajhadin, M. Mazloum-Ardakani, A. Amini, Metal oxide-based gas sensors for detection of exhaled breath markers. Med Devices Sens, e10161 (2020)
287. L. Xu, R. Zheng, S. Liu, J. Song, J. Chen, B. Dong, H. Song, NiO@ZnO heterostructured nanotubes: coelectrospinning fabrication, characterization, and highly enhanced gas sensing properties. Inorg Chem **51**(14), 7733–7740 (2012)
288. C. Fan, F. Sun, X. Wang, Z. Huang, M. Keshvardoostchokami, P. Kumar, B. Liu, Synthesis of ZnO hierarchical structures and their gas sensing properties. Nanomater **9**(9), 1277 (2019)
289. P. Li, S. Yu, H. Zhang, Preparation and performance analysis of Ag/ZnO humidity sensor. Sensors (Basel) **21**(3), 857 (2021)
290. Z. Lu, Q. Zhou, C. Wang, Z. Wei, L. Xu, Y. Gui, Electrospun ZnO-SnO_2 composite nanofibers and enhanced sensing properties to SF6 decomposition byproduct H_2S. Front Chem **6**, 540 (2018)
291. D. Zhang, G. Dong, Y. Cao, Y. Zhang, Ethanol gas sensing properties of lead sulfide quantum dots-decorated zinc oxide nanorods prepared by hydrothermal process combining with successive ionic-layer adsorption and reaction method. J Colloid Interface Sci **528**, 184–191 (2018)
292. Y.T. Tsai, S.J. Chang, L.W. Ji, Y.J. Hsiao, I.T. Tang, H.Y. Lu, Y. L. Chu, High sensitivity of NO gas sensors based on novel Ag-doped ZnO nanoflowers enhanced with a UV light-emitting diode. ACS Omega **3**(10), 13798–13807 (2018)
293. K. Suematsu, K. Watanabe, A. Tou, Y. Sun, K. Shimanoe, Ultraselective toluene-gas sensor: nanosized gold loaded on zinc oxide nanoparticles. Anal Chem **90**(3), 1959–1966 (2018)
294. W. Guo, B. Zhao, Q. Zhou, Y. He, Z. Wang, N. Radacsi, N, Fe-doped ZnO/reduced graphene oxide nanocomposite with synergic enhanced gas sensing performance for the effective detection of formaldehyde. ACS Omega **4**(6), 10252–10262 (2019)
295. S. Wang, W. Chen, J. Li, Z. Song, H. Zhang, W. Zeng, Low working temperature of ZnO-MoS_2 nanocomposites for delaying aging with good acetylene gas-sensing properties. Nanomaterials **10, 1902**(10) (2020)
296. G.H. Mhlongo, D.E. Motaung, F.R. Cummings, H.C. Swart, S.S. Ray, A highly responsive NH_3 sensor based on Pd-loaded ZnO nanoparticles prepared via a chemical precipitation approach. Sci Rep **9**(1), 9881 (2019)
297. V. Platonov, M. Rumyantseva, N. Khmelevsky, A. Gaskov, Electrospun ZnO/Pd nanofibers: CO sensing and humidity effect. Sensors (Basel) **20**(24), 7333 (2020)
298. M. Mascini, S. Gaggiotti, F. Della Pelle, C. Di Natale, S. Qakala, E. Iwuoha, P. Pittia, D. Compagnone, Peptide modified ZnO nanoparticles as gas sensors array for volatile organic compounds (VOCs). Front Chem **6**, 105 (2018)
299. M. Hjiri, L. El Mir, S.G. Leonardi, N. Donato, G. Neri, CO and NO_2 selective monitoring by ZnO-based sensors. Nanomaterials. **3**(3), 357–369 (2013)
300. W. Chen, Q. Li, L. Xu, W. Zeng, Gas sensing properties of ZnO-SnO_2 nanostructures. J Nanosci Nanotechnol **15**(2), 1245–1252 (2015)
301. C. Han, X. Li, Y. Liu, X. Li, C. Shao, J. Ri, J. Ma, Y. Liu, Construction of In_2O_3/ZnO yolk-shell nanofibers for room-temperature NO2 detection under UV illumination. J Hazard Mater **403**, 124093 (2021)
302. Y. Wang, X.N. Meng, J.L. Cao, Rapid detection of low concentration CO using Pt-loaded ZnO nanosheets. J Hazard Mater **381**, 120944 (2020)
303. A. Chizhov, M. Rumyantseva, A. Gaskov, Light activation of nanocrystalline metal oxides for gas sensing: principles, achievements, challenges. Nanomater **11**(4), 892 (2021)
304. Y.H. Zhang, Y.L. Li, F.L. Gong, K.F. Xie, H.L. Zhang, S.M. Fang, Double-platelet Pd@ZnO microcrystals for NO_2 chemical sensors: their facile synthesis and DFT investigation. Phys Chem Chem Phys **21**(39), 22039–22047 (2019)
305. A. Umar, M.A. Khan, R. Kumar, H. Algarni, Ag-doped ZnO nanoparticles for enhanced ethanol gas sensing application. J Nanosci Nanotechnol **18**(5), 3557–3562 (2018)
306. A. Chanda, S. Gupta, M. Vasundhara, S.R. Joshi, G.R. Mutta, J. Singh, Study of structural, optical and magnetic properties of cobalt doped ZnO nanorods. RSC Adv **7**, 50527–50536 (2017)
307. N. Aggarwal, K. Kaur, A. Vasisth, N.K. Verma, Synthesis and characterization of Gd-doped ZnO nanorods. AIP Conf Proc **2050**, 020015-1–020015-5 (2018)
308. P. Thamaraiselvan, S. Kannan, S. Gowthaman, M. Kutraleeswaran, Preparation and characterization of Mn doped ZnO nanorods. Int J S Res Sci Tech **4**, 679–685 (2018)

309. B. Kumar, J.K. Tiwari, S. Ghosh, Multiferrocity in vanadium doped ZnO. AIP Conf Proc **2265**, 030304 (2020)
310. P.G. Undre, P.B. Kharat, J.S. Kounsalye, R.V. Kathare, K.M. Jadhav, Structural, morphological and magnetic properties of Cu^{2+} doped ZnO nanoparticles. J Phys Conf Ser **2020**, 012008 (**1644**)
311. H. Li, M. Xia, K. Luo, P.W. Wang, Influence of Pr^{3+} doping on the microstructure of ZnO quantum dots. J Wuhan Univ Technol Mater Sci Ed **30**, 16–21 (2015)
312. S. Hernández, D. Hidalgo, A. Sacco, A. Chiodoni, A. Lamberti, V. Cauda, E. Tresso, G. Saracco, Comparison of photocatalytic and transport properties of TiO_2 and ZnO nanostructures for solar-driven water splitting. Phys Chem Chem Phys **17**(12), 7775–7786 (2015)
313. Z.C. Zhao, C.L. Yang, Q.T. Meng, M.S. Wang, X.G. Ma, $ZnCdO_2$ monolayer — a complex 2D structure of ZnO and CdO monolayers for photocatalytic water splitting driven by visible-light. Spectrochim Acta A Mol Biomol Spectrosc **230**, 118068 (2020)
314. S. Shawuti, A.U.R. Sherwani, M.M. Can, M.A. Gülgün, Complex impedance analyses of Li doped ZnO electrolyte materials. Sci Rep **10**(1), 8228 (2020)
315. J. Li, H. Yuan, J. Li, W. Zhang, Y. Liu, N. Liu, H. Cao, Z. Jiao, The significant role of the chemically bonded interfaces in BiVO4/ZnO heterostructures for photoelectrochemical water splitting. Appl Catal B Environ **285**, 119833 (2021)
316. J. Jiang, J. Pi, J. Cai, The advancing of zinc oxide nanoparticles for biomedical applications. Bioinorg Chem Appl **2018**, 1–18 (2018)
317. A. Sirelkhatim, S. Mahmud, A. Seeni, N.H.M. Kaus, L.C. Ann, S. K.M. Bakhori, D. Mohamad, Review on zinc oxide nanoparticles: antibacterial activity and toxicity mechanism. Nano-Micro Letters **7**(3), 219–242 (2015)